σ^{28}-dependent small RNAs regulate timing of flagella biosynthesis

Sahar Melamed[1,2,*], Aixia Zhang[1], Michal Jarnik[1], Joshua Mills[1,3], Hongen Zhang[4] and Gisela Storz[1,5,*]

[1]Division of Molecular and Cellular Biology, Eunice Kennedy Shriver National Institute of Child Health and Human Development, Bethesda, MD 20892-5430, USA.

[2]Present address: The Faculty of Medicine, The Hebrew University of Jerusalem, Jerusalem, Israel.

[3]Present address: Max Planck Institute for Marine Microbiology, Bremen, Germany.

[4]Bioinformatics and Scientific Computing Core, Eunice Kennedy Shriver National Institute of Child Health and Human Development, Bethesda, MD 20892-5430, USA.

[5]Lead Contact.

[*]Correspondence. E-mail: sahar.melamed@mail.huji.ac.il (S.M.), storzg@mail.nih.gov (G.S.)

SUMMARY

Flagella are important for bacterial motility as well as for pathogenesis. Synthesis of these structures is energy intensive and, while extensive transcriptional regulation has been described, little is known about the posttranscriptional regulation. Small RNAs (sRNAs) are widespread posttranscriptional regulators, most base pairing with mRNAs to affect their stability and/or translation. Here we describe four UTR-derived sRNAs (UhpU, MotR, FliX and FlgO) whose expression is controlled by the flagella sigma factor σ^{28} (*fliA*) in *Escherichia coli*. Interestingly, MotR and FliX have opposing effects on flagellin protein levels, flagella number and cell motility, with MotR accelerating flagella synthesis and FliX decelerating flagella synthesis. Unlike most sRNAs, MotR and FliX base pair within the coding sequences of target mRNAs. They also uniquely act on ribosomal protein mRNAs thus coordinating flagella synthesis with ribosome production. The study shows how sRNA-mediated regulation can overlay a complex network enabling nuanced control of flagella synthesis.

Keywords: Hfq, post-transcriptional regulation, S10, RIL-seq, *fliA*

INTRODUCTION

Most bacteria are motile and can swim through liquid and semiliquid environments in large part driven by the flagellum. The highly complex bacterial flagellum consists of three major domains: an ion-driven motor, which can provide torque in either direction; a universal joint called the hook-basal body, which transmits motor torque; and a 20 nm thick hollow filament tube composed of the flagellin subunit, which acts as a propeller (reviewed in (Altegoer & Bange, 2015, Nakamura & Minamino, 2019)). The flagellum structure is comprised of many proteins, and the flagellar regulon encompasses more than 50 genes. Since it is estimated that one flagellum constitutes ~2% of the total protein in the cell, synthesis is a very expensive process requiring extensive use of ribosomes (reviewed in (Soutourina & Bertin, 2003, Guttenplan & Kearns, 2013)).

To ensure that flagellar components are made in the order in which they are needed, transcription of the genes in the regulon is activated in a sequential manner in *Escherichia coli* (Kalir *et al.*, 2001) and *Salmonella enterica* (reviewed in (Chevance & Hughes, 2008)). The genes can be divided into three groups based on their time of activation: early genes, middle genes, and late genes (Figure 1A). The FlhDC transcription regulators, encoded by the two early genes, activate the transcription of the middle genes, which are responsible for building the hook-basal body. FlhDC also induce *fliA*, encoding sigma factor σ^{28} (Fitzgerald *et al.*, 2014). σ^{28} in turn activates transcription of the late genes responsible for completing the flagellum and the chemotaxis system, and enhances the activation of many of the middle genes. σ^{28} activity itself is negatively regulated by the anti-sigma factor, FlgM, which is transported out of the cell when hook-basal body synthesis is complete (reviewed in (Smith & Hoover, 2009, Osterman *et al.*, 2015). Given the numerous components required at different times and different stoichiometries

during flagellum assembly, various factors can be rate limiting under specific conditions (reviewed in (Chevance & Hughes, 2008)). The dependence of flagella synthesis on FlhDC and σ^{28} generates a coherent feed-forward loop. In this loop, the first regulator (FlhDC) activates the second regulator (σ^{28}), and they both additively activate their target genes. This results in prolonged flagellar expression, protecting the flagella synthesis from a transient loss of input signal (Kalir *et al.*, 2005).

Since flagella are so costly to produce, synthesis is tightly regulated such that flagellar components are only made when motility is beneficial. Thus, flagellar synthesis is strongly impacted by environmental signals. For instance, flagellar gene expression is decreased in the presence of D-glucose, in high temperatures, high salt, and extreme pH as well as the presence of DNA gyrase inhibitors (Shi *et al.*, 1993, Adler & Templeton, 1967). The flagellar genes are activated under oxygen-limited conditions (Landini & Zehnder, 2002) and at various stages of infection by bacterial pathogens (reviewed in (Erhardt, 2016)). Consequently, transcription of many genes in the flagellar regulon is regulated in response to a range of environmental signals. For example, transcription of *flhDC* is controlled by at least 13 transcription factors, each of them active under different conditions (reviewed in (Prüß, 2017)).

While the activation of flagella synthesis has been examined in some detail, there has been less investigation into the termination of synthesis, which we presume is equally important for the conservation of resources. Additionally, while transcriptional regulation of flagella genes has been studied for many years, less is known about the post-transcriptional control of the regulon. Small RNAs (sRNAs) are short RNA transcripts that can originate from many different genetic loci (reviewed in (Adams & Storz, 2020)) and are key post-transcriptional regulators in bacteria. They usually regulate their targets in trans via limited base-pairing, affecting translation

and/or mRNA stability (reviewed in (Hör *et al.*, 2020)). Many characterized sRNAs are stabilized and their base pairing with targets increased by RNA chaperones, of which the hexameric, ring-shaped Hfq protein has been studied most extensively (reviewed in (Updegrove *et al.*, 2016, Holmqvist & Vogel, 2018)). The only post-transcriptional control by base pairing sRNAs described for the *E. coli* flagellar regulon thus far is negative regulation of *flhDC* by ArcZ, OmrA, OmrB and OxyS (De Lay & Gottesman, 2012) and positive regulation of the same mRNA by McaS (Thomason *et al.*, 2012). These sRNAs and a few other sRNAs also were shown to affect motility and biofilm formation (Bak *et al.*, 2015).

Herein we characterize four σ^{28}-dependent sRNAs, which were detected with their targets on Hfq through RIL-seq methodology that captures the sRNA-target interactome (Melamed *et al.*, 2016, Melamed *et al.*, 2020). These sRNAs originate from the untranslated regions (UTRs) of mRNAs, three of which belong to the flagella regulon. We identified a wide range of targets for the sRNAs, including genes related to metabolism, flagella synthesis, and ribosome synthesis and observed that the sRNAs act on some of these targets by unique modes of action. We show that three of these sRNAs regulate flagella number and bacterial motility, imposing temporal control of flagella synthesis and likely integrating additional metabolic signals into this complex regulatory network.

RESULTS

σ^{28}-dependent sRNAs are expressed sequentially in log phase

Analysis of several different RNA-seq data sets suggested the expression of four σ^{28}-dependent sRNAs (Melamed *et al.*, 2016, Fitzgerald *et al.*, 2014, Thomason *et al.*, 2015, Melamed *et al.*, 2020). These sRNAs originate from the UTRs of protein coding genes (Figures 1B and S1A). UhpU corresponds to the 3´ UTR of *uhpT*, which encodes a hexose phosphate transporter (Marger & Saier, 1993). UhpU is transcribed from its own promoter inside the coding sequence (CDS) of *uhpT* (Thomason *et al.*, 2015). The other three σ^{28}-dependent sRNAs correspond to the UTRs of the late genes in the flagellar regulon. MotR originates from the 5´ UTR of *motA*, which encodes part of the flagellar motor complex. Based on previous transcription start site analysis, the promoter for *motR* is within the *flhC* CDS and also is the promoter of the downstream *motAB-cheAW* operon (Thomason *et al.*, 2015, Fitzgerald *et al.*, 2014). FliX originates from the 3´ UTR of *fliC*, which encodes flagellin, the core component of the flagellar filament (reviewed in (Thomson *et al.*, 2018)). FlgO originates from the 3´ UTR of *flgL*, a gene that encodes a junction protein shown to connect the flagella to the hook in *S. enterica* (Ikeda *et al.*, 1987). The observation that FliX and FlgO levels decline substantially in RNA-seq libraries treated with 5´ phosphate-dependent exonuclease to deplete processed RNAs (Thomason *et al.*, 2015), indicates that both of these sRNAs are processed from their parental mRNAs.

Northern blot analysis confirmed σ^{28}-dependent synthesis of these sRNAs since expression was significantly decreased in a mutant lacking σ^{28} (Δ*fliA*) (Figure 1C). Given that most σ^{28} -dependent mRNAs encode flagella components, the σ^{28} regulation of the sRNAs suggests they impact flagella synthesis. The northern analysis also showed that the levels of the four σ^{28}-dependent sRNAs are highest in the transition from mid-exponential to stationary phase

growth, though there are some differences with UhpU and MotR peaking before FliX and FlgO (Figure 1C). Since flagellar components are expressed at precise times, the difference in the UhpU and MotR peak times compared to the FliX and FlgO peak times hints at different roles for each of these sRNAs in flagella synthesis. For UhpU, two predominant bands were observed, a long transcript and a shorter transcript processed from UhpU (denoted UhpU-S), which corresponds to the higher peak in the sequencing data (Figure 1B). One prominent band was detected for MotR and FliX, while a doublet was observed for FlgO. Additional higher bands detected by the MotR probe can be explained by RNA polymerase read through of the MotR terminator into the downstream *motAB-cheAW* operon, while the additional bands seen for FliX can be explained by alternative processing of the *fliC* mRNA.

The predicted structures for the four σ^{28}-dependent sRNAs (Figure S1B), with strong stem-loops at the 3´ ends, are consistent with the structures of known Hfq-binding sRNAs and the Hfq binding observed in the RIL-seq data. To confirm Hfq binding, we isolated RNA that co-immunoprecipitated with Hfq (Figure 1D). The same prominent bands, but fewer background bands, were detected for three of the sRNAs; ~260 nt and ~60 nt bands for UhpU and UhpU-S, respectively, a ~95 nt band for MotR, and a doublet of ~75 nt bands for FlgO. For FliX, we detected the same ~200 nt band as well as a second ~100 nt FliX band (denoted FliX-S; Figure S1A) that corresponds to the 3´ peak in the sequencing data (Figure 1B).

We also examined the levels of the four sRNAs in minimal media (M63) supplemented with different carbon sources (Figure S1C). Generally, the sRNAs levels in minimal medium are comparable to their levels in rich media (LB) with the exception of medium with glucose 6-phosphate (G6P), where the levels of UhpU-S are elevated while the levels of full-length UhpU transcript and the other σ^{28}-dependent sRNAs are decreased. These observations suggest an

alternative means for UhpU-S generation from the *uhpT* mRNA known to be induced by G6P (Verhamme *et al.*, 2001). We also observe more FliX products, particularly for cells grown in minimal medium with ribose or galactose.

σ^{28}-dependent sRNAs impact flagella number and bacterial motility

To begin to decipher the roles of the four σ^{28}-dependent sRNAs, we constructed plasmids for IPTG-inducible and constitutive overexpression of the sRNAs (Figure S2). Given that it was challenging to obtain constructs constitutively overexpressing UhpU because all clones had mutations, this sRNA could only be expressed from the IPTG-inducible promoter. We also constructed plasmids overexpressing MotR*, a more abundant derivative of MotR identified by chance (TGC at positions 6-8 mutated to GAG; Figure S1A).

We tested the effects of overexpressing the sRNAs on flagellar synthesis by determining the number of flagella by electron microscopy and on bacterial motility by swimming assays. Intriguingly, the individual sRNAs had different effects. UhpU overexpression caused a moderate increase in flagella number (Figure 2A) and a marked increase in motility (Figure 2B). Overexpression of MotR, particularly MotR*, led to a dramatic increase in the flagella number (Figure 2C) and a moderate increase in motility (Figure 2D). In contrast to UhpU and MotR, FliX overexpression led to a reduction in the number of flagella, an effect that was enhanced in a strain overexpressing FliX-S (Figure 2E). Overexpression of FliX-S also reduced bacterial motility (Figure 2F). FlgO overexpression did not result in a detectable effect on flagella number or motility (Figures 2G and 2H). The WT *E. coli* strain used throughout the paper is highly motile due to an IS1 insertion in the *crl* gene, thus eliminating expression of a protein that promotes σ^{S} binding to the RNA polymerase core enzyme (Typas *et al.*, 2007), resulting in

higher expression of the flagellar regulatory cascade (Pesavento *et al.*, 2008). However, the less motile strain with the restored *crl*$^{+}$ gene was used to assess the UhpU and MotR effects on motility, given that no effects were observed with the highly motile *crl*$^{-}$ strain. Together these results show that the σ^{28}-dependent sRNAs have a range of effects on the number of flagella and motility, with UhpU and MotR, which are expressed first, increasing both phenotypes and FliX, which is expressed later, decreasing both.

σ^{28}-dependent sRNAs have wide range of potential targets based on RIL-seq analysis

To understand the phenotypes associated with overexpression of the σ^{28}-dependent sRNAs expression, we took advantage of the sRNA-target interactome data obtained by RIL-seq (Melamed *et al.*, 2020, Melamed *et al.*, 2016). We analyzed RIL-seq data generated from 18 samples representing six different growth conditions (Table S1). The sRNAs differ significantly in their target sets (Figure S3A), but, interestingly, the *fliC* gene encoding flagellin was present in the target sets of UhpU, MotR, and FliX (Figures 3A and S3A). Particularly striking was the large number of chimeras between the 3´ end of *fliC* corresponding to FliX (blue) and the 5´ coding sequence of *fliC* (red).

In general, UhpU is a hub with hundreds of RIL-seq targets under the tested conditions. Its target set comprised a wide range of genes, including multiple genes that have roles in flagella synthesis and carbon metabolism. MotR and FliX were associated with fewer targets, but uniquely, both sets were enriched for genes encoding ribosomal proteins (Table S1). Although FlgO is one of the most strongly enriched sRNAs upon Hfq purification (ranked fourth in Melamed et al., 2020), it had the smallest set of targets, and almost none of the targets were

found in more than two conditions, hinting FlgO might not act as a conventional Hfq-dependent base-pairing sRNA.

UhpU, MotR and FliX impact flagellin levels

Given the high number of chimeras between UhpU, MotR, and FliX and the flagellin mRNA *fliC*, we first examined the consequences of overexpressing these sRNAs on the levels of the flagellin protein and *fliC* mRNA. We observed somewhat increased levels of flagellin, both as cytosolic monomers (Figure 3B) and de-polymerized flagella (Figure S3B) with UhpU and MotR* overexpression while no flagellin was detected with FliX-S overexpression. These differences are reflected in increased levels of the *fliC* mRNA with overexpression of UhpU, particularly in a *crl*$^{+}$ background, and overexpression of MotR*, particularly at OD_{600} ~0.2 (Figure 3C). In contrast, *fliC* mRNA levels were decreased with FliX-S overexpression. The impacts of the sRNAs on flagellin protein and *fliC* mRNA levels are consistent with the increased flagella number upon UhpU or MotR overexpression and decreased flagella number upon FliX overexpression. Since the MotR and FliX sRNAs had the most striking effects on flagella number and unique ribosomal protein gene targets, we decided to focus on these two sRNAs for the rest of the study.

MotR and FliX have opposite effects on the expression of middle and late flagella genes

While MotR and FliX had clear effects on flagella number and motility (Figure 2), no flagellar genes other than *fliC* were top RIL-seq targets for either MotR or FliX. Thus, we examined the impact of overexpressing these sRNAs on the transcriptome by RNA-seq analysis (Table S2). The transcripts whose levels increased most with MotR* overexpression compared to the vector

control (Figure 4A) corresponded predominantly to late genes and, to a lesser extent, middle genes, of the flagellar regulon. Of the 91 genes whose expression increased ≥2-fold by MotR*, 26 are reduced ≥2-fold in a strain lacking σ^{28} (Δ*fliA*) (Fitzgerald *et al.*, 2014) (Figure S3C). Additionally, the sequence motif found for the promoters of the genes for which expression increased ≥2 fold (Figure S3D) is nearly identical to a σ^{28} recognition motif (Fitzgerald *et al.*, 2014). These observations indicate that MotR overexpression leads to an upregulation of flagellar genes. The MotR sRNA effect on the flagellar genes is not dependent on the anti-σ^{28} factor (FlgM), which represses σ^{28} activity, since, despite the expected overall increase in flagella number in the Δ*flgM* background, MotR* overexpression led to still higher numbers of flagella (Figure S4A). We also examined the levels of C-terminally SPA-tagged FlhD, FlgJ and CheW, representing early, middle, and late genes, respectively. We found increased levels of both FlgJ and CheW upon MotR* overexpression, particularly early in growth, consistent with a positive effect of MotR on flagella synthesis (Figure 4B).

Opposite to what was observed for MotR*, transcripts for flagellar genes were reduced by FliX-S overexpression (Figure 4C). More specifically, 35 out of 41 genes for which the expression is reduced ≥2 fold are middle or late genes of the flagella regulon. The reduction also was observed for SPA tagged FlgJ and CheW proteins. We also detected a moderate reduction in the levels of tagged FlhD (Figure 4D). Thus, in contrast to MotR, FliX has a negative effect on flagella synthesis.

MotR upregulates S10 ribosomal protein levels

Given that ribosomal protein coding genes were almost exclusively found in chimeras with MotR and FliX and no other sRNAs, we decided to further investigate MotR and FliX regulation

of these genes. Several of the top interactions for MotR and FliX in the RIL-seq data mapped to genes in the essential S10 operon (Table S1 and Figure S3A). The co-transcriptional regulation of the S10 operon has been studied extensively (Zengel & Lindahl, 1996, Zengel *et al.*, 2002, Zengel & Lindahl, 1992). The leader sequence upstream of the first gene *rpsJ* encoding S10 is bound by the ribosomal protein L4, encoded by the third gene in the operon (*rplD*), causing transcription termination, thus modulating the levels of all the ribosomal proteins in the operon in response to the levels of unincorporated L4. L4 binding also has been shown to inhibit translation of *rpsJ*, an effect that can be genetically distinguished from the L4 effect on transcription termination (Freedman *et al.*, 1987).

The RIL-seq data showed that MotR interacts with *rpsJ* (Figure 5A). To examine the effect of MotR on *rpsJ* expression, we fused the S10 leader and part of the *rpsJ* CDS, including the position of the RIL-seq *rpsJ*-MotR chimeras and the region of predicted base-pairing (Figure 5B), to a GFP reporter (Corcoran *et al.*, 2012, Urban & Vogel, 2009). MotR overexpression elevated the levels of the *rpsJ-gfp* fusion, and MotR* enhanced this effect (Figure 5C). Positive regulation of S10 expression was similarly observed by immunoblot analysis of an N-terminal FLAG-tagged S10 protein encoded along with the S10 leader behind the heterologous promoter on a pBAD plasmid (Figure 5D). A mutation in the MotR seed sequence (MotR-M1, Figure S1A) eliminated the up-regulation of the FLAG-tagged S10 (Figure 5D) and reduced the flagella number (Figure S4B). As a further test for direct base pairing between MotR and the sequences internal to the *rpsJ* CDS, we carried out in vitro structure probing in the presence of Hfq (Figure S5A and S5B). The RNase and lead cleavage assays supported the position of the predicted base-pairing between MotR and *rpsJ* mRNA, indicating MotR binds to *rpsJ* in its CDS. Strong binding of Hfq to the attenuator hairpin (Stem E in Figure 5E) also was noted in the S10 leader

sequence (Figure S5B). This region has three ARN sequences (AGG, AGU and AAC), known to be important for Hfq binding to mRNAs (reviewed in (Updegrove *et al.*, 2016)).

Most characterized positive regulation by Hfq-binding sRNAs occurs through base pairing in 5´ leader sequences (Papenfort & Vanderpool, 2015). Thus, we wondered how base pairing of MotR with sequences internal to the *rpsJ* CDS resulted in increased S10 levels. We hypothesized that MotR binding could modulate L4 and/or Hfq binding to S10 leader sequences. Given that a prematurely terminated mRNA would not have the site the MotR binding site, the internal MotR binding should not directly affect transcription termination. We hypothesize an MotR effect on L4 and/or Hfq binding instead promotes *rpsJ* translation.

To define the sequence determinants critical for MotR-mediated up regulation, we generated a series of *rpsJ-gfp* fusions (Figure 5E). We generated fusions to several different truncations to include only the first seven amino acids of S10 removing the MotR base pairing site, to remove the S10 leader sequence, to remove stem D required for L4-mediated regulation, or to remove the attenuator hairpin stem E. MotR-dependent regulation was eliminated for each of these constructs suggesting that the MotR binding site internal to *rpsJ* CDS and the S10 leader sequence are needed for MotR dependent regulation (Figure 5F). To further test if Hfq binding to *rpsJ* is critical for the activation, we repeat the GFP reporter assay in an Hfq^{Y25D} mutant defective for binding ARN sequences on the distal face of the protein (Zhang *et al.*, 2013a). Consistent with an Hfq role, MotR, which is present at the same levels in an Hfq WT and in the Hfq^{Y25D} mutant (Figure S5C), no longer upregulates *rpsJ-gfp* in the distal face mutant background (Figure 5F). Collectively, our results are consistent with MotR base pairing affecting L4 and Hfq binding resulting in increased translation of *rpsJ* yielding higher S10 levels.

S10 affects flagella number through its anti-terminator function

Intrigued by the fact that MotR induced S10, we decided to examine the impact of elevated S10 protein levels on flagella number. The S10 protein has two roles in the cell. It is incorporated into the 30S ribosome subunit but also forms a transcription anti-termination complex with NusB, primarily binding to the Box A sequences of *rrn* operons (Lüttgen *et al.*, 2002, Luo *et al.*, 2008). We evaluated the importance of each of two roles to flagella number by electron microscopy. First, we overexpressed an S10 mutant (S10Δloop) that is missing the ribosome binding loop but is still active in anti-termination (Luo *et al.*, 2008) from an inducible plasmid and analyzed the number of flagella per cell. Cells carrying S10Δloop plasmid had higher number of flagella, similarly to the phenotype observed with MotR* overexpression (Figure 5G). Next, we tested the effect of MotR* overexpression in a strain that cannot form the S10-NusB anti-termination complex. We used a Δ*nusB* strain since S10 is essential and cannot be deleted. In this background, the stimulatory effect of MotR* on flagella number was eliminated (Figure 5H). Expression of S10Δloop in Δ*nusB* background similarly did not lead to an increase in the number of flagella (Figure S4C). Altogether, these data suggest that anti-termination by S10-NusB complex is important for flagella synthesis.

We noted that overexpression of wild type S10 from the plasmid used to overexpression S10Δloop did not lead to an increase in flagella number (Figure 5G), though presumably MotR is normally increasing flagella number by impacting the levels of the WT protein. Possibly, only a very specific concentration of S10 relative to other ribosome proteins increases the S10 role as an anti-terminator. Alternatively, there may be other factors regulating the fate of S10 that did not impact S10 overexpressed from the plasmid.

Based on all of these observations, we propose that increased levels of non-ribosome associated S10 leads to increased levels of the S10-NusB anti-termination complex associated with the RNA polymerase-σ^{28} complex and increased antitermination of the long operons encoding flagellar proteins. It is also conceivable that even a slight upregulation of the S10 operon, as well as the S6 operon given a significant number of MotR-*rpsF* chimeras (Table S1), along with antitermination of *rrn* operons, could lead to more active ribosomes, which are needed for flagellar protein synthesis.

FliX downregulates the S10 ribosomal protein operon

Based on the RIL-seq data, FliX interacts with multiple regions in the S10 operon mRNA, all internal to the CDSs (Figure 6A). The predicted base-pairing regions (Figure 6B) align with the highest peaks of chimeras in the RIL-seq data and overlap with the seed sequence suggested for FliX (Melamed *et al.*, 2016). We tested the effects of FliX on expression from this operon by constructing *gfp* fusions to regions of *rplC*, *rpsQ*, and *rpsS*-*rplV*. In all cases, overproduction of FliX or FliX-S led to a reduction in the expression of these fusions (Figure 6C). To confirm a direct interaction between FliX and the *rpsS* mRNA, we carried out structure probing (Figure S6). The regions that were changed in *rpsS* and FliX in the in-vitro footprinting aligned with the predicted binding region between the two RNAs.

We hypothesized that the downregulation of the *rplC*, *rpsQ*, and *rpsS*-*rplV* fusions by FliX is due to mRNA degradation. Consistent with this hypothesis, in vivo primer extension assays carried out for RNA isolated from in mid-log phase cells (OD_{600} ~0.6) revealed an increase in 5´ ends, presumably due to cleavage, in close proximity to the binding site on *rpsS* mRNA in FliX or FliX-S overexpressing strains (Figure 6D). The negative effect of FliX on

ribosomal components, which could reduce the number of active ribosomes, is consistent with the general repressive role of this sRNA. We note that we did not observe differential expression of the S10 transcript in the RNA-seq analysis (Figure 4C and Table S2) carried out for RNA isolated from cells earlier in growth (OD_{600} ~0.2), suggesting FliX may be more effective later in growth. It is also conceivable that the S10 mRNA reciprocally regulates FliX connecting ribosomal protein and flagella synthesis.

MotR accelerates and FliX decelerates flagella synthesis

The preceding observations indicated that MotR overexpression leads to increased expression of flagellar genes and elevated levels of flagellin and ribosomal proteins, while FliX has the opposite effect. To examine the consequences of chromosomally-encoded MotR and FliX on the flagella regulon and flagella synthesis, we introduced the three-nucleotide M1 substitutions in the seed sequences of *motR* and *fliX* (FliX-M1, Figure S1A) at their endogenous chromosomal positions, avoiding the disruption of the nearby genes. MotR-M1 RNA levels were somewhat lower than WT MotR levels (Figure S5C). The prominent ~200 nt FliX band also was reduced for FliX-M1, while other FliX processing products were less effected (Figure S6C). As MotR and FliX overexpression had clear effects on FlgJ-SPA levels (Figures 4B and 4D), we assessed the impact of *motR* and *fliX* chromosomal mutants on this fusion. Western analysis in the *motR-M1* strain in comparison to its parental WT revealed a delayed initiation of FlgJ-SPA synthesis in the mutant (Figure 7A). In contrast, FlgJ-SPA levels in the *fliX-M1* strain increased compared to the parental WT strain (Figure 7B). The *motR-M1* chromosomal mutation also was associated with a moderate reduction in flagella number at two time points (OD_{600} ~ 0.6 and 2.0) (Figure

7C), while slightly higher numbers of flagella were observed for the *fliX-M1* strain at the later time point (OD_{600} ~ 2.0) (Figure 7D).

Next, we compared the motility of the *motR-M1* and *fliX-M1* strains to WT strains by mixing strains transformed with plasmids expressing either GFP or mCherry. WT strains expressing GFP were mixed with *motR-M1* or *fliX-M1* cells expressing mCherry or vice versa, and their motility was compared in a swimming assay. For both combinations of WT and *motR-M1,* the fluorescent signal produced by the WT strain spread further on the plate in comparison to the fluorescent signal generated by *motR-M1* mutant (Figure 7E). This suggests that the *motR-M1* mutant exhibits reduced motility compared to the WT strain. No significant difference was observed between WT and *fliX-M1* in the swimming assay (Figure S6D). Since flagella can play roles in different modes of *E. coli* locomotion, we additionally tested if the *motR-M1* and *fliX-M1* mutations had an effect on swarming; a coordinated translocation of a bacterial cells across solid or semi-solid surfaces (reviewed in (Kearns, 2010)). Interestingly, WT cells swarm better than *fliX-M1* cells (Figure 7F) while the *motR-M1* mutation had the opposite effect, with increased swarming compared to the WT cells (Figure S5D).

Collectively these observations indicate that MotR, expressed early in growth, accelerates flagella synthesis by positively regulating the middle and the late genes, while FliX, whose levels peak later, decelerates flagella synthesis by downregulating the flagella regulon, mainly the middle and the late genes. MotR and FliX thus add another layer of regulation to the flagella regulon, integrating it with the synthesis of ribosomal components (Figure 7G).

DISCUSSION

In this study, we describe four *E. coli* sRNAs whose expression is dependent on σ^{28}. We found three of these sRNAs affect flagella number and bacterial motility. Although previous studies showed that base pairing sRNAs act on the *flhDC* mRNA (Thomason *et al.*, 2012, De Lay & Gottesman, 2012), our results revealed that the effect of sRNAs on flagellar synthesis is far more pervasive. Intriguingly, two of the σ^{28}-dependent sRNAs show opposite effects. MotR, expressed earlier in growth, increases expression of flagellar and ribosomal proteins along with flagella number, while FliX, expressed later in growth, decreases expression of these proteins and flagella number. Thus, the two sRNAs, respectively, serve as an accelerator and decelerator for flagellar synthesis.

Non-canonical mechanisms of sRNA action

Most commonly, sRNAs base pair with the 5´ UTRs of mRNA targets or at the very beginning of the CDS, primarily affecting the ribosome binding or mRNA stability. However, MotR and FliX bind in the middle or even close to the ends of their target CDSs in the S10 operon. Interestingly, for this operon, the consequences of MotR and FliX overexpression are different. MotR, which base pairs internal to *rpsJ*, appears to affect the S10 leader sequence, yielding higher expression of the S10 protein, whereas FliX, which base pairs internal to *rpsS*, leads to degradation of the mRNA. We note that significant RIL-seq signal for the MotR and FliX interaction with the *fliC* mRNA also is internal to the coding sequence and speculate that the respective positive and negative effects of the sRNAs may occur by similar mechanisms for this gene. Based on RIL-seq data, more examples of this type of interaction remain to be characterized.

Given that our study made extensive use of RIL-seq data, it provides an opportunity to evaluate these data. While RIL-seq provides a comprehensive map of RNA-RNA interactions that take place on Hfq under a specific condition, some caution about the interpretation is warranted as the interactions represent multiple types of relationships between two RNAs. As was found by a recent study (Faigenbaum-Romm *et al.*, 2020), we suggest that if an interaction is highly abundant and discovered under multiple conditions, the sRNA is more likely to have a regulatory impact on the target mRNA. We noticed that the spread of the RIL-seq signal varies significantly between targets. One possible explanation for multiple peaks and a broad distribution is more than one base pairing site for the sRNA on the mRNA but this hypothesis requires further investigation. We predict additional studies of sRNA-target pairs with different types of RIL-seq signals will give further insights into the steps and outcomes of base pairing.

The most studied and conserved sRNA-binding protein in gram-negative bacteria is Hfq. However, there are other sRNA-binding proteins (reviewed in (Melamed, 2020)). Among these is ProQ, which was shown to have overlapping, complementary, and competing roles with Hfq in *E. coli* (Melamed *et al.*, 2020). Interestingly, ProQ was found to affect motility and chemotaxis *S. enterica* (Westermann *et al.*, 2019). In the absence of ProQ, the target sets for the σ^{28}-dependent sRNAs on Hfq were changed significantly in *E. coli* (Table S5 in (Melamed *et al.*, 2020)) suggesting that competition between Hfq and ProQ for binding RNAs likely also influences this regulatory circuit. In this context, it is worth noting that FlgO, the fourth σ^{28}-dependent sRNA, which originates from the 3'UTR of the *flgL* and strongly binds Hfq, does not have many targets. Possibly, FlgO has a role in titrating Hfq from other sRNAs or proteins, or in the recruitment of other proteins to a complex with Hfq.

Conservation of σ^{28}-dependent sRNAs

We were surprised to find so many σ^{28}-dependent Hfq-binding sRNAs and wondered about the distribution. A previous study assessing the conservation of the *motR* and *uhpU* promoters showed that, while the *motR* promoter is well conserved across proteobacteria species, the *uhpU* promoter was not, implying on different evolutionary pressures (Fitzgerald *et al.*, 2018). Interestingly, however, a sRNA termed RsaG, that originates from the 3' UTR of *uhpT* and also is induced by glucose-6-phosphate, was found in the Gram-positive bacterium, *Staphylococcus aureus* (Bronesky *et al.*, 2019). Although there is no sequence similarity between UhpU and RsaG, and RsaG has not been reported to regulate flagella synthesis, the independent evolution of a regulatory sRNAs at the 3´ UTR of *uhpT* in two disparate bacterial species is intriguing.

The σ^{28}-dependent sRNAs themselves are conserved among some of the Enterobacteriaceae (Figure S7) and thus may play a role in pathogenicity. It is likely that still other sRNA regulators of the flagella regulon remain to be characterized. In a recent study of *S. enterica*, a leader RNA originated from the *mgtCBR* virulence operon was shown to affect the synthesis of one of the two flagellin genes that exist in this bacterium, impacting virulence and motility (Choi *et al.*, 2017).

Roles of σ^{28}-dependent sRNAs

The UhpU RIL-seq target set includes many flagellar regulon genes and some transcription regulators of the flagellar regulon, such as LrhA (Lehnen *et al.*, 2002), hinting at a mechanism by which UhpU can affect flagella number and bacterial motility. However, since UhpU can also be derived from the *uhpT* mRNA (Figure S1C) and is predicted to have many targets that participate in carbon and nutrient metabolism (Table S1), we suggest this sRNA may play a broader role in

linking carbon metabolism with flagella synthesis and motility. This role could be crucial for *E. coli* competition with other bacteria for resources in their natural habitat.

MotR and FliX each have a much more limited target sets but comprise a unique regulatory toggle. The transcription of the two sRNA is dependent on the same sigma factor, and they base pair in the CDS of targets in the same operons, but their binding results in opposing regulation. MotR, which is transcribed from within *flhC* at the top of the flagella regulon, reaches its highest levels earlier than FliX and accelerates the flagella synthesis, while FliX, which is cleaved from the mRNA required to make the last protein needed to complete the flagellum, reaches its highest levels later in growth and appears to decelerate flagella synthesis. This regulation has interesting differential consequences for *E. coli* motility; the chromosomal *motR-M1* mutation resulted in reduced swimming but increased swarming whereas the chromosomal *fliX-M1* mutation resulted in reduced swarming.

Both sRNAs modulate flagella synthesis by regulating the levels of both flagellar and ribosomal proteins. The effect on ribosomal proteins is noteworthy because no other sRNAs have been found to target these operons. While FliX simply directs the cleavage of the S10 mRNA, MotR is unique in that binding leads to higher levels of the S10 protein, which has a second function in antitermination. We speculate that MotR activation of S10 expression could serve an autoregulatory role. Early in growth, transcription initiating from the σ^{28}-dependent promoter in *flhC* terminates 3´ of *motR*. As MotR levels increase, there is a concomitant increase in S10 levels, which could promote antitermination of this transcript and increased readthrough leading to decreased MotR levels and increased full-length *motRAB-cheAW* mRNA.

In general, the σ^{28}-dependent sRNAs form a new level of regulation in the flagellar regulon and reinforce the fact that flagella synthesis is exquisitely regulated. The regulon serves

as a model of a temporally-controlled regulatory network with contributions from both transcription factors and regulatory RNAs.

AUTHOR CONTRIBUTIONS

S.M. and G.S. conceived of the project. S.M., A.Z. and J.M. designed, performed, and analyzed the experiments. M.J. performed all electron microscopy. H.Z. performed all the computational analyses under the supervision of S.M. S.M., A.Z. and G.S. prepared the figures and wrote the manuscript. G.S. supervised the project.

DECLARATION OF INTERESTS

The authors declare no competing interests.

ACKNOWLEDGEMENTS

We thank M. Gottesman for plasmids expressing wild type and *rpsJ* mutants, O. Steele-Mortimer for plasmids constitutively expressing GFP or mCherry, and D. Court for the S10 antibody. We thank J. Wade for sharing the sequences used to generate the σ^{28} binding motif and J. Wade and G. Baniulyte for advice on the FRUIT method. We thank the NICHD Molecular Genomics Core, particularly Tianwei Li, for all the library sequencing. We also appreciate the help of A. Peer with the sRNA conservation analysis. We are grateful to the Storz and S. Gottesman labs for all of the helpful discussions and thank the Storz lab, S. Gottesman and J. Wade for their comments on the manuscript. This work was supported by the Intramural Research Program of the *Eunice Kennedy Shriver* National Institute of Child Health and Human Development.

MAIN FIGURE TITLES AND LEGENDS

Figure 1. σ^{28}-dependent sRNAs are primarily expressed in log phase

(A) Overview of the flagella regulon. The early genes initiate the transcription of the middle genes, including *fliA* which encodes σ^{28}. In turn, σ^{28} initiates the transcription of the late genes and enhances the transcription of some of the middle genes. For the middle and late genes, only selected operons are shown. The sRNAs analyzed in this study are colored in blue. This model was inspired by (Kalir *et al.*, 2005).

(B) Browser images showing levels of UhpU, MotR, FliX and FlgO sRNAs in total RNA (black) and Hfq co-immunoprecipitation (gray) libraries. Normalized read count ranges are shown in the upper right of each frame. Data analyzed is from (RIL-seq experiment 1, Melamed *et al.*, 2020).

(C) Northern blot analysis of total RNA from WT (MG1655) or Δ*fliA* cells grown to the indicated time points. The same membrane was probed for all four σ^{28}-dependent sRNAs. A full-length transcript (~260 nt) and several processed transcripts, of which one is predominant (UhpU-S, ~60 nt), are detected for UhpU, one prominent band (~95 nt) is detected for MotR, one prominent band (~200 nt) is detected for FliX, and two close bands close in size (~75 nt) are detected for FlgO.

(D) WT (GSO983) cells were grown to OD_{600} ~0.6 and ~1.0. RNA was extracted from total lysates as well as samples from co-immunoprecipitation with Hfq, separated on an acrylamide gel, transferred to a membrane, and probed for σ^{28}-dependent sRNAs. A ~100 nt FliX band (FliX-S) was revealed immunoprecipitating with Hfq.

In both (C) and (D), RNAs were probed sequentially on the same membrane and 5S RNA served as a loading control.

Figure 2. Overexpression of the σ^{28}-dependent sRNAs leads to differences in flagella number and motility

(A) Increase in flagella number with UhpU overexpression based on electron microscopy analysis for WT cells carrying an empty vector or overexpressing UhpU.

(B) Increased motility with UhpU overexpression based on swimming assay in soft agar (0.3%) for WT (*crl*$^{+}$) cells carrying an empty vector or overexpressing UhpU.

(C) Increase in flagella number with MotR or MotR* overexpression based on electron microscopy analysis for WT cells carrying an empty vector or overexpressing MotR or MotR*.

(D) Increased motility with MotR* overexpression based on swimming assay in soft agar (0.3%) for WT (*crl*$^{+}$) cells carrying an empty vector or overexpressing MotR*.

(E) Reduction in flagella number with FliX or FliX-S overexpression based on electron microscopy analysis for WT cells carrying an empty vector or overexpressing FliX or FliX-S.

(F) Reduced motility with FliX-S overexpression based on swimming assay in soft agar (0.3%) for WT (*crl*$^{-}$) cells carrying an empty vector or overexpressing FliX-S.

(G) No change in flagella number with FlgO overexpression based on electron microscopy analysis for WT cells carrying an empty vector or overexpressing FlgO.

(H) No change in motility with FlgO overexpression based on swimming assay in soft agar (0.3%) for WT (*crl*$^{-}$) cells carrying an empty vector or overexpressing FlgO.

Cells in (A), (B), (D), (F), (G) and (H) were induced with 1 mM IPTG. Quantification for all the assays is shown on the right.

For (A), (C), (E) and (G) quantification of the number of flagella per cell was done by counting the flagella for 20 cells (black dots), and a two-way ANOVA comparison was performed to calculate the significance of the change in flagella number (ns = not significant, ** = P<0.01,

**** = P<0.0001). The experiments presented in (C) and (E) were carried out on same day, and the same pZE sample is shown.

Graphs for (B), (D), (F) and (H) show the average of three biological repeats. Error bars represent one SD.

Figure 3. Multiple sRNAs regulate flagellin synthesis

(A) Browser image showing chimeras (red and blue) for UhpU, MotR, and FliX at the *fliCX* region. Data analyzed is from (RIL-seq experiment 1, Melamed *et al.*, 2020). Red and blue lines indicate the RNA in the region is first or second RNA in the chimera, respectively.

(B) Immunoblot analysis showing UhpU and MotR overexpression leads to increased flagellin levels and FliX overexpression leads to reduced flagellin levels. Flagellin levels were determined by immunoblot analysis using α-FliC antibody. A sample from a Δ*fliC* strain was included as a control given the detection of a cross-reacting band slightly larger than flagellin. The Ponceau S-stained membrane serves as a loading control.

(C) Northern blot analysis showing UhpU and MotR* overexpression increases *fliC* mRNA levels and FliX-S overexpression reduces *fliC* levels. 5S RNA served as a loading control. A *crl*$^{+}$ background was used for the UhpU overexpressing cells.

Figure 4. MotR* and FliX-S overproduction leads to increased and decreased expression of flagella genes, respectively

(A) MotR* induces σ^{28}-dependent genes. Dots outside of the diagonal lines correspond to RNAs that increase or decrease by ≥ 2-fold. Green dots indicate σ^{28}-dependent RNAs.

(B) MotR increases the levels of SPA tagged FlgJ and CheW. FlhD-SPA, FlgJ-SPA and CheW-

SPA levels across growth in the presence of MotR* expressed from pZE plasmid were determined by immunoblot analysis using α-FLAG antibody.

(C) FliX reduces middle and late genes of the flagella regulon. Dots outside of the diagonal lines correspond to RNAs that increase or decrease by ≥ 2-fold. Red dots indicate the flagella regulon genes.

(D) FliX reduces the levels of SPA tagged FlhD, FlgJ and CheW. FlhD-SPA, FlgJ-SPA and CheW-SPA levels across growth in the presence of FliX-S expressed from pZE plasmid were determined by immunoblot analysis using α-FLAG antibody.

For (A) and (C), WT harboring the control vector or the MotR* or the FliX-S expression plasmid were grown to OD_{600} ~ 0.2; total RNA was extracted and used for the construction of cDNA libraries, which were analyzed as described in STAR Methods.

For (B) and (D), the Ponceau S-stained membrane serves as a loading control.

Figure 5. MotR base pairs with the S10 mRNA leading to upregulation of S10

(A) Browser image showing MotR chimeras (in red) in S10 leader and *rpsJ* region. Data analyzed is from (RIL-seq experiment 1, Melamed *et al.*, 2020). Coverage of the region in total RNAseq libraries is shown for empty vector (pZE) and for pZE-MotR* overexpression (Table S2). The Hfq and MotR binding sites as detected in Figure S5A and S5B are highlighted in light blue.

(B) Base-pairing between *rpsJ* and MotR.

(C) MotR induces *rpsJ-gfp* reporter fusion. Test of *rpsJ*-MotR interaction with reporter assays of *rpsJ-gfp* expressed from pXG10-SF with MotR or MotR* expressed from pZE.

(D) MotR increases FLAG tagged S10 levels. 3xFLAG-S10 was expressed from pBAD33 and

MotR or MotR* was expressed from pZE. A mutation in MotR eliminates this regulation. 3xFLAG-S10 levels were determined by immunoblot analysis using α-FLAG antibody. The Ponceau S-stained membrane serves as a loading control.

(E) S10 leader sequence and secondary structure based on (Zengel *et al.*, 2002). Hfq binding region is highlighted in blue. *rpsJ* start codon is labeled in green. The first boxed letters represent S10 leader terminator, and the second boxed letters represent the Shine-Dalgarno sequence. Lines represent the parts of the sequences that were assayed in the GFP reporter assay in panel F.

(F) MotR induces *rpsJ-gfp* levels only when the S10 leader and MotR binding sites are present. Reporter assays of various *rpsJ-gfp* fusions expressed from pXG10-SF with MotR* expressed from pZE.

(G) MotR* and S10Δloop overexpression similarly increase the number of flagella. The number of flagella per cell detected by electron microscopy were counted for WT cells harboring the indicated plasmids.

(H) MotR effect is eliminated in Δ*nusB* background. The number of flagella per cell detected by electron microscopy were counted for WT or Δ*nusB* cells harboring the indicated plasmids.

For (C) and (F), the average of three independent measurements is shown. Error bars represent one SD.

For (G) and (H), flagella were counted for 20 cells (black dots), and a two-way ANOVA comparison was performed to calculate the significance of the change in flagella number (ns = not significant, **** = P<0.0001).

Figure 6. FliX base pairs with the S10 mRNA leading to downregulation

(A) Browser image showing FliX chimeras (in red) in the S10 operon. Highlighted in light blue are the base pairing regions between FliX and the S10 operon mRNA. Data analyzed is from (RIL-seq experiment 1, Melamed *et al.*, 2020).

(B) Base pairing between *rplC, rpsS, rpsQ* and FliX. Underlined is the seed sequence of FliX based on Melamed et al., 2016.

(C) Test of FliX interactions with reporter assays of *rplC-gfp, rpsS-rplV-gfp* and *rpsQ-gfp* expressed from pXG10-SF or pXG30-SF with FliX or FliX-S expressed from pZE. The average of three independent measurements is shown. Error bars represent one SD.

(D) *rpsS* mRNA is cleaved upon FliX overexpression. Total RNA was extracted from WT or Δ*fliCX* strains harboring the indicated plasmids at OD_{600} ~ 0.6 and then subject to primer extension analysis using a primer hybridizing downstream of FliX binding site on *rpsS*.

Figure 7. Complex regulatory network of sRNAs controlling the initiation of flagella synthesis

(A) Reduction in FlgJ-SPA levels in a *motR-M1* mutant. SPA tagged FlgJ levels across growth in WT (GSO1081) and in *motR-M1* mutant (GSO1082) were monitored.

(B) Increase in FlgJ-SPA levels in a *fliX-M1* mutant. SPA tagged FlgJ levels across growth in WT (GSO1080) and in *fliX-M1* mutant (GSO1083) were monitored.

(C) Reduction in flagella number in a *motR-M1* mutant.

(D) Increase in flagella number in a *fliX-M1* mutant.

(E) Reduced motility in *motR-M1* mutant (GSO1087) based on a swimming competition assay with its corresponding WT (GSO1088). The indicated mixed cultures were spotted on a soft agar (0.3%) plate, incubated at 30˚C, and imaged after 18 h.

(F) Reduced swarming in *fliX-M1* mutant (GSO1076) based on a swarming competition assay with its corresponding WT (GSO983). The indicated mixed cultures were spotted on a soft agar (0.6%) plate, incubated at 30˚C for 48 h, then moved to 37˚C for additional 24 h and imaged.

(G) σ^{28}-dependent sRNAs control flagella synthesis at different levels. MotR activates the middle and the late genes expression. FliX downregulates expression of the middle and late genes. MotR and FliX also connect ribosome and flagella synthesis by regulating genes in the S10 operon.

In (A) and (B), FlgJ-SPA levels were determined by immunoblot analysis using α-FLAG antibody. The Ponceau S-stained membrane serves as a loading control.

In (C) and (D), the number of flagella per cell detected by electron microscopy were counted for for 40 cells (black dots) for the WT, *motR-M1* and *fliX-M1* strains at three points in growth (OD_{600} ~ 0.2, OD_{600} ~ 0.6, and OD_{600} ~ 2.0). A two-way ANOVA comparison was performed to calculate the significance of the change in flagella number (ns = not significant, * = $P<0.05$, ** = $P<0.01$, *** = $P<0.001$).

For (E) and (F), WT or the corresponding mutant, expressed either green fluorescent signal or red fluorescent signal by carrying pCON1.proC-GFP or pCON1.proC-mCherry plasmid, respectively. In the left images, WT cells expressing GFP were mixed with mutant cells expressing mCherry; in the middle images, WT cells expressing mCherry were mixed with mutant cells expressing GFP; in the right images, WT cells expressing GFP were mixed with WT cells expressing mCherry.

STAR METHODS

CONTACT FOR REAGENT AND MATERIALS AVAILABILITY

Further information and requests for resources and reagents should be directed to and will be fulfilled by the Lead Contact, Gisela Storz (storzg@mail.nih.gov).

All unique/stable reagents generated in this study are available from the Lead Contact with a completed Materials Transfer Agreement.

EXPERIMENTAL MODEL AND SUBJECT DETAILS

Bacterial strains, oligonucleotides and plasmids

E. coli MG1655 (GSO982 or GSO983) or MC4100 (GSO614) strains served as the WT strains in this study. All other bacterial strains used in this study are listed in the Table S3. *E. coli* K-12 MG1655 genome was used as template to amplify mRNAs and sRNAs to be cloned into their respective sites. Unless indicated otherwise, all strains were grown with shaking at 250 rpm at 37°C in LB rich medium. Ampicillin (100 µg/ml), chloramphenicol (25 µg/ml), kanamycin (30 µg/ml), arabinose (0.2%) and IPTG (1 mM) were added where appropriate. Unless indicated otherwise, overnight cultures were diluted to an OD_{600} = 0.05 and grown for the indicated times or to the desired optical densities.

METHOD DETAILS

Strain construction

fliA::kan, *fliCX::kan*, and *fliX-M1:kan* strains were constructed by amplifying the kan^R sequence from pKD4 (Datsenko & Wanner, 2000) using oligonucleotides listed in Table S3 and recombining (Datsenko & Wanner, 2000) the product into the chromosome of strain NM400

(kind gift of Nadim Majdalani). *flgJ* was SPA-tagged by amplifying the SPA sequence adjacent to *kan*^{R} sequence from pJL148 (Zeghouf *et al.*, 2004) using oligonucleotides listed in Table S3 and recombining (Datsenko & Wanner, 2000) the product into the chromosome of strain NM400. *motR-M1* strain was constructed using the scar-free system, FRUIT (Stringer *et al.*, 2012) as previously described. Briefly, *thyA* was deleted from MG1655 (*crl*$^-$) (GSO983) strain by PCR amplification of Δ*thyA* from AMD061 (Stringer *et al.*, 2012) followed by recombination using pKD46 (Datsenko & Wanner, 2000). Next, *thyA* was inserted back to the genome next to the site of mutation and selection was made by growth on minimal media lacking thymine. The *motR-M1* mutation was introduced while simultaneously removing *thyA*. The selection for colonies missing *thyA* was carried out using minimal medium M9 plates supplied with 0.4% glucose, 0.2% casamino acids, 20 µg/ml trimethoprim, and 100 µg/ml thymine. *flgM::kan* and *nusB::kan* deletion strains were obtained from other groups (Baba *et al.*, 2006) as referenced in Table S3. All deletions and mutations were confirmed by sequencing and then transferred to new backgrounds by P1 transduction. Where indicted, *kan*^{R} was removed from the chromosome using plasmid pCP20 (Cherepanov & Wackernagel, 1995).

Plasmid construction

Descriptions of plasmids used in this study are in Table S3. Construction of the constitutive overexpression plasmids was done according to (Urban and Vogel, 2009) using pZE12-luc. The IPTG-inducible UhpU overexpression plasmid was constructed using a pBRplac derivative harboring *kan*^{R}, pMSG14 (Guo *et al.*, 2014). The *uhpU* sequence, starting from its second nt, was amplified by PCR using primers TU558 and TU561 (Table S3), digested with *Aat*II and *Hin*dIII and cloned into pMSG14 digested with the same restriction enzymes. IPTG-inducible MotR and

FliX IPTG overexpressing plasmids were constructed using the pBRplac-lacI derivative, pNM46 (kind gift of Nadim Majdalani). For the pNM46 constructs, the insert sequences were amplified by PCR using primers as indicated in Table S3, digested with *Aat*II and *Eco*RI and cloned into pNM46 digested with the same restriction enzymes. 3xFLAG-*rpsJ* was expressed from pBAD33 (Guzman *et al.*, 1995). The S10 leader and *rpsJ* sequence along with the 3xFLAG sequence was PCR amplified using primers SM533 and SM435, digested with *Kpn*I and *Hin*dIII and cloned into pBAD33 digested with the same restriction enzymes. Construction of GFP-fusion plasmids was carried out principally as described in (Urban and Vogel, 2009), using the pXG10-SF or pXG30-SF (Corcoran et al., 2012). Briefly, regions of target genes, mainly regions captured in the chimeric fragments, were PCR amplified, digested with *Mph*1103I and *Nhe*I and cloned into pXG10-SF or pXG30-SF digested with the same restriction enzymes. The full list of oligonucleotides used in this study can be found in Table S3. Mutagenesis of the different plasmids was achieved using the QuikChange Lightning Site-Directed Mutagenesis Kit (Agilent). All plasmids were freshly transformed into the appropriate strains before each of the experiments.

RNA isolation

Cells corresponding to the equivalent of 10-20 OD_{600} were collected, washed once with 1X PBS, and frozen in liquid nitrogen. RNA was extracted according to the standard TRIzol protocol (Thermo Fisher Scientific) as described previously (Melamed *et al.*, 2020). At the last step, RNA was resuspended in 20-50 µl of DEPC water and quantified using a NanoDrop (Thermo Fisher Scientific).

Northern blot analysis

For smaller RNAs, total RNA (5 μg) was separated on a denaturing 8% polyacrylamide urea gel containing 6 M urea (1:4 mix of Ureagel Complete to Ureagel-8 (National Diagnostics) with 0.08% ammonium persulfate) in 1X TBE buffer at 300V for 90 min. The RNA was transferred to a Zeta-Probe GT membrane (Bio-Rad) at 20 V for 16 h in 0.5X TBE. For longer RNAs, total RNA (10 μg) were fractionated on formaldehyde-MOPS agarose gels as previously described (Adams *et al.*, 2017). Briefly, RNA was denatured in 3.7% formaldehyde (Fisher), 1X MOPS (20 mM MOPS, 5 mM NaOAc, 1 mM EDTA, pH 7.0) and 1X RNA loading dye (Thermo Fisher Scientific) for 10 min at 70°C and incubated on ice. The RNA was loaded onto a 2% NuSieve 3:1 agarose (Lonza), 1X MOPS, 2% formaldehyde gel and separated at 125-150V at 4°C for 1-2 h and then transferred to a Zeta-Probe GT membrane (Bio-Rad) via capillary action overnight (Streit *et al.*, 2009). For both types of blots, the RNA was crosslinked to the membranes by UV irradiation. RiboRuler High Range and Low Range RNA ladders (Thermo Fisher Scientific) were marked by UV-shadowing. Oligonucleotide probes (listed in Table S3) for the different RNAs were labelled with 0.3 mCi of [γ-^{32}P] ATP (Perkin Elmer) by incubating with 10 U of T4 polynucleotide kinase (New England Biolabs) at 37°C for 1 h.

Translational reporter assay

The GFP reporter assay was carried out essentially as described previously (Melamed et al., 2016). Overnight cultures were grown in 2 ml LB media supplemented with the appropriate antibiotics at 37°C with constant shaking at 250 rpm. Cells were then diluted into 1 ml fresh LB medium supplemented with the appropriate antibiotics in 96-well plate and grown at 37°C with constant shaking at 250 rpm for 3 h. Cells were pelleted and resuspended in filtered 1 X PBS.

Fluorescence was measured using the BD LSRFortessa or Beckman Coulter Cytoflex flow cytometer. The level of regulation was calculated by subtracting the auto-fluorescence and then calculating the ratio between the fluorescence signal of a strain carrying the sRNA over-expressing plasmid and the signal of a strain carrying the control plasmid. Three biological repeats were prepared for every sample. IPTG (1 mM) was added to cells harboring inducible sRNAs plasmids.

Immunoblot analysis

Bacteria were grown to the desired OD_{600}, and the cells in 0.5 ml – 4 ml of culture were collected. Cell lysates were prepared by resuspending cell pellets with SDS-loading buffer normalized to the cell density, and samples were then heated for 10 min at 95°C. Protein samples were subjected to a 4%-15% polyacrylamide SDS gel electrophoresis followed by electrotransfer to a nitrocellulose membrane (Fisher Scientific). The membrane was blocked with 3% milk, probed with anti-flagellin antibodies (1/10,000) (Abcam) and then with anti-rabbit secondary antibody (1/10,000) or with ANTI-FLAG M2-Peroxidase (HRP) (1/1,000), (Sigma-Aldrich). Signals were visualized by the ECL system (Biorad).

RNA structure probing

GeneBlock fragments carrying the *motR*, *fliX*, *rpsJ* or *rpsS* CDS (IDT) were used as DNA templates for in vitro transcription with MEGAshortscript T7 High Yield Transcription Kit (Invitrogen). The transcripts were dephosphorylated with calf intestinal alkaline phosphatase (CIP, New England Biolabs) and then radioactively labeled at 5' end with [γ-^{32}P] ATP (Perkin Elmer) and T4 kinase (Invitrogen), and purified on an 8% polyacrylamide/7M urea gel and

eluted in buffer containing 20 mM Tris-HCl/pH 7.5, 0.5 M NaOAc, 10 mM EDTA and 1% SDS at 4°C for overnight, followed by ethanol precipitation. The RNA concentration was determined by measuring the OD_{260} on Nanodrop.

For all the structural probing assays, 0.2 pmole of the labeled transcript, 2 pmole of unlabeled transcript and 1 µg of yeast RNA with or without 2 pmole (hexameric concentration) of purified Hfq were mixed in 10 µl of 1x Structural Buffer in Ambion RNase T1 Kit (Invitrogen). The reactions were incubated at 37°C for 10 min, followed by treatment at 37°C with 0.02 U RNase T1 for 10 min, 1.3 U RNase III for 1.5 min, or 50 µmole lead acetate for 10 min, whereupon 20 µl Inactivation Buffer and 1 µl Glycoblue were added. The RNAs were precipitated and resuspended in 10 µl Loading Buffer, and analyzed on a 8% polyacrylamide/7 M urea gel run in 1x TBE. RNase T1 and alkali digestion ladders of the end-labeled transcripts were used as molecular size markers.

Flagellin measurements during filament assembly.

WT (GSO983) cells harboring pBR*, pBR*-UhpU, pZE, pZE-MotR, pZE-MotR*, pZE-FliX or pZE-FliX-S were grown with shaking at 180 rpm in 5 ml of LB at 37°C to OD_{600} ~ 1.0. Cell pellets collected by centrifugation were suspended in 5 ml PBS and then heated at 65°C for 5 min, followed by centrifugation to obtain the cell pellets and supernatants, which contained the cytoplasmic flagellin molecules and depolymerized flagellin monomers, respectively. The cell pellets were resuspended in the SDS-loading buffer, normalized to the cell density. Proteins in the supernatants were precipitated by 10% trichloroacetic acid, suspended in Tris/SDS loading buffer and heated at 95°C for 10 min.

RNA coimmunoprecipitation (Co-IP) assay

RNAs that co-IP using polyclonal antibodies to Hfq were isolated as described (Zhang *et al.*, 2002) with the following modifications. MG1655 (GSO983) was grown to OD_{600} ~0.6 and ~1.0 in LB medium. Cells corresponding to the equivalent of 20 OD_{600} were collected, and cell lysates were prepared by vortexing with 212-300 µm glass beads (Sigma-Aldrich) in a final volume of 1 ml lysis buffer (20 mM Tris-HCl/pH 8.0, 150 mM KCl, 1 mM $MgCl_2$, 1 mM DTT). Co-IPs were carried out using 100 ml of α-Hfq, 120 mg of protein A-Sepharose beads (GE Healthcare), and 950 µl of cell lysate. Co-IP RNA was isolated from protein A-Sepharose beads by extraction with phenol: chloroform:isoamyl alcohol (25:24:1), followed by ethanol precipitation. Total RNA was isolated from 50 ml of cell lysate by TRIzol (Thermo Fisher Scientific) extraction followed by chloroform extraction and isopropanol precipitation. Total and co-IP RNA samples were resuspended in 15 µl of DEPC H_2O, and 5 µg total RNA and 0.5 µg co-IP RNA were subjected to northern analysis as described above.

Primer extension assay

Primer extension analysis was performed using an oligonucleotide (listed in Table S3) specific to the *rpsS* as described (Zhang *et al.*, 1998). RNA samples (5 µg of total RNA) were incubated with 2 pmol of 5-^{32}P-end-labeled primer at 80°C and then slow-cooled to 42°C. After the addition of dNTPs (1 mM each) and AMV reverse transcriptase (10 U, Life Sciences Advanced Technologies Inc.), the reactions were incubated in a 10-µl reaction volume at 42°C for 1 h. The reactions were terminated by adding 10 µl of Stop Loading Buffer. The cDNA products then were fractionated on 8% polyacrylamide urea gels containing 8 M urea in 1X TBE buffer at 70 W for 70 min.

Analysis of flagella number by electron microscopy

Overnight cultures were diluted in fresh medium and grown with shaking at 180 rpm, at 37°C to mid-log phase (OD_{600}~0.6-0.8) unless indicated otherwise. Cells were collected by centrifugation at 1,000 rpm for 20 min, and pellet was resuspended in 300 µl of saline. Next, 3 µl of bacterial suspension were placed on a freshly glow-discharged carbon covered electron microspical (EM) support grid (EMS, Hatfield, PA) for 5 min. The grid was washed twice with distilled water and stained for 1 min with 0.75% aqueous solution of uranyl formate, pH 4.5. The grids were imaged in Thermo Fisher Scientific (Hillsboro, OR) FEI Tecnai 20 electron microscope operated at 120 kV. The images were recorded using AMT (Woburn, MA) XR81 CCD camera. Flagella were counted for 20-40 cells in each sample as indicated in the figure legends. Each analysis was repeated a minimum of three times.

Swimming and swarming assays

For the swimming assay, overnight cultures (~1 µl) were spotted onto 0.3% soft agar plate by touching the agar softly with the tip and ejecting the culture. Plates were incubated with the agar at the bottom at 30°C above a beaker filled with water for 9-24 h. Plates were made with the appropriate antibiotics and with 1 mM IPTG. The plates were imaged using Bio-Rad imager (using Colorimetric settings) and the diameter of the bacterial culture was calculated using the ImageJ software. Two technical repeats and three biological repeats were carried out for each strain.

The swimming or swarming competition assays were done in a similar why as described above with the following adjustments. Cells were first transformed with pCON1.proC-GFP or

pCON1.proC-mCherry plasmids (Cooper *et al.*, 2017), resulting in a GFP or an mCherry signal, respectively. In each case, equal numbers of bacterial cells based on OD_{600} of each overnight culture for one strain expressing a green fluorescence signal and a second strain expressing a red fluorescent signal were mixed before spotting them onto the soft agar plate, 0.3% agar for a swimming assay and 0.6% for a swarming assay. For the swimming assays, plates were incubated as described above, for the swarming assays, plates were incubated at 30°C for 48 h and then moved to 37°C for additional 24 h. Images were taken using Bio-Rad imager with the following settings: Colorimetric (1-2 sec) for bright field, Cy2 for GFP (auto optimal exposure), Cy3 for mCherry (auto optimal exposure). Images were merged using Image Lab (Bio-Rad).

RNAseq

Overnight cultures were diluted in fresh LB medium and grown to early-log phase (OD_{600}~0.2). RNA was extracted using the standard TRIzol protocol (Thermo Fisher Scientific) as described above. Total RNA libraries were constructed using the RNAtag-Seq protocol with a few modifications to allow capture of short RNA fragments as previously described (Melamed *et al.*, 2018). The libraries were sequenced by paired-end sequencing using the HiSeq 2500 system (Illumina). RNA-seq data processing follows the same procedures as RIL-seq data analysis for QC analysis, adaptor removal, and alignment with the Python RILSeq package (Melamed *et al.*, 2018). Sequences were mapped using annotation files based on EcoCyc version 20.0 (Keseler *et al.*, 2013) with manual addition of sRNAs and small proteins from (Hör *et al.*, 2020).

Recognition of sequence motifs

Common binding motifs were searched with MEME software (Bailey *et al.*, 2009). For each transcription unit, genomic sequence was extracted using coordinates for 500 nt upstream to the transcription start site and 100 nt downstream of the transcription start site. Overlapping sequences were merged as one and all ‘‘T’’ bases were replaced by ‘‘U’’. For outputs, motif length was restricted to 28.

Functional annotation analysis

Functional annotation analysis of sRNAs targets was carried out using the Database for Annotation, Visualization and Integrated Discovery (DAVID) (Huang da *et al.*, 2009). Gene names served as the input list in each case. Targets that were present in at least three RIL-seq conditions in Table S1 were included in the analysis.

QUANTIFICATION AND STATISTICAL ANALYSIS

Circos plots

Circos plots follow the procedures of R RCircos Package (Zhang *et al.*, 2013b). Link lines are used to label the statistically significant chimeric fragments (S-chimeras as defined in (Melamed *et al.*, 2016)). RIL-seq from six different growth conditions was analyzed and S-chimeras present in at least four of the six conditions are included in the plots.

Browser images

Data from RIL-seq experiment 1 from Melamed at al., 2020 extracted for unified S-chimeras files for the different sRNAs were mapped based on the first nt of each read in the chimera. BED files are generated with Python RILSeq package (Melamed *et al.*, 2018) and viewed using the

UCSC genome browser (Kent *et al.*, 2002). For previously annotated RNA in GTF file, BED files are directly generated with command of generate_BED_file_of_endpoints.py and EcoCyc ID. For genes annotated in the current study, significant chimeras which involve the relevant gene are first extracted from significant interaction file, then chimeric reads involving the S-chimeras are extracted from chimeric read file. To be a qualified chimeric read, RNA1 start position of the read must overlap with the genomic range of RNA1 in S-chimera and RNA2 start position of the read must overlap with the genomic range of RNA2 in S-chimera. Finally, the read list for genes annotated in the current study is supplied to generate_BED_file_of_endpoints.py command to generate BED file.

DATA AND CODE AVAILABILITY

The sequencing data reported in this paper have been deposited in GEO under accession number GSE1774487.

SUPPLEMENTAL TABLES

Supp. Table S1. Target sets of σ^{28}-dependent sRNAs based on RIL-seq datasets (related to Figures 3, 5, 6 and S3)

RIL-seq datasets from experiments done in 6 different conditions (Melamed *et al.*, 2020, Melamed *et al.*, 2016) were analyzed in order to generate a target set for each of the four sRNAs. Tables are sorted according to the number of conditions in which a target was found. sRNAs targets functional annotation analysis was done using DAVID. Targets that were present in at least three RIL-seq conditions in were included in the analysis. The top annotation cluster is shown for each dataset.

Supp. Table S2. RNA levels in different RNAseq datasets (related to Figures 4 and S3)

Total RNA libraries reads were normalized by the library total number of reads (RPM). For MotR* data, average expression of three biological repeats was calculated for the uninduced MotR* strain (pZE) and for the MotR* overexpressing strain (pZE-MotR*). For FliX-S data, average expression of two biological repeats was calculated for the uninduced FliX-S strain (pZE in repeat 1 and pBR-lacI-FliX-S with 0 mM IPTG in repeat 2) and for the FliX-S overexpressing strain (pZE-FliX-S in repeat 1 and pBR-lacI-FliX-S with 1 mM IPTG in repeat 2). For Δ*fliA* data, average expression of two biological repeats was calculated for the WT strain and for the Δ*fliA* strain. Fold change for each RNA was calculated by dividing average expression in the control strain, with the average expression in the overexpression (MotR* or FliX-S) or deletion (Δ*fliA*) strain.

Supp. Table S3. List of deoxyribonucleotides, strains, and plasmids used in this work (for STAR methods)

REFERENCES

Adams, P.P., Flores Avile, C., Popitsch, N., Bilusic, I., Schroeder, R., Lybecker, M., and Jewett, M.W. (2017) In vivo expression technology and 5' end mapping of the *Borrelia burgdorferi* transcriptome identify novel RNAs expressed during mammalian infection. *Nucleic Acids Res.* **45**: 775-792.

Adams, P.P., and Storz, G. (2020) Prevalence of small base-pairing RNAs derived from diverse genomic loci. *Biochim. Biophys. Acta Gene Regul. Mech.* **1863**: 194524.

Adler, J., and Templeton, B. (1967) The effect of environmental conditions on the motility of *Escherichia coli*. *J. Gen. Microbiol.* **46**: 175-184.

Altegoer, F., and Bange, G. (2015) Undiscovered regions on the molecular landscape of flagellar assembly. *Curr. Opin. Microbiol.* **28**: 98-105.

Baba, T., Ara, T., Hasegawa, M., Takai, Y., Okumura, Y., Baba, M., Datsenko, K.A., Tomita, M., Wanner, B.L., and Mori, H. (2006) Construction of *Escherichia coli* K-12 in-frame, single-gene knockout mutants: the Keio collection. *Mol. Syst. Biol.* **2**: 2006.0008.

Bailey, T.L., Boden, M., Buske, F.A., Frith, M., Grant, C.E., Clementi, L., Ren, J., Li, W.W., and Noble, W.S. (2009) MEME SUITE: tools for motif discovery and searching. *Nucleic Acids Res.* **37**: W202-W208.

Bak, G., Lee, J., Suk, S., Kim, D., Young Lee, J., Kim, K.S., Choi, B.S., and Lee, Y. (2015) Identification of novel sRNAs involved in biofilm formation, motility, and fimbriae formation in *Escherichia coli*. *Sci. Rep.* **5**: 15287.

Bronesky, D., Desgranges, E., Corvaglia, A., François, P., Caballero, C.J., Prado, L., Toledo-Arana, A., Lasa, I., Moreau, K., Vandenesch, F., Marzi, S., Romby, P., and Caldelari, I. (2019) A multifaceted small RNA modulates gene expression upon glucose limitation in *Staphylococcus aureus*. *EMBO J.* **38**: e99363.

Cherepanov, P.P., and Wackernagel, W. (1995) Gene disruption in *Escherichia coli*: TcR and KmR cassettes with the option of Flp-catalyzed excision of the antibiotic-resistance determinant. *Gene* **158**: 9-14.

Chevance, F.F., and Hughes, K.T. (2008) Coordinating assembly of a bacterial macromolecular machine. *Nat. Rev. Microbiol.* **6**: 455-465.

Choi, E., Han, Y., Cho, Y.-J., Nam, D., and Lee, E.-J. (2017) A trans-acting leader RNA from a *Salmonella* virulence gene. *Proc. Natl. Acad. Sci. USA* **114**: 10232-11023.

Cooper, K.G., Chong, A., Starr, T., Finn, C.E., and Steele-Mortimer, O. (2017) Predictable, tunable protein production in *Salmonella* for studying host-pathogen interactions. *Front. Cell Infect. Microbiol.* **7**: 475.

Corcoran, C.P., Podkaminski, D., Papenfort, K., Urban, J.H., Hinton, J.C., and Vogel, J. (2012) Superfolder GFP reporters validate diverse new mRNA targets of the classic porin regulator, MicF RNA. *Mol. Microbiol.* **84**: 428-445.

Datsenko, K.A., and Wanner, B.L. (2000) One-step inactivation of chromosomal genes in *Escherichia coli* K-12 using PCR products. *Proc. Natl. Acad. Sci. USA* **97**: 6640-6645.

De Lay, N., and Gottesman, S. (2012) A complex network of small non-coding RNAs regulate motility in *Escherichia coli*. *Mol. Microbiol.* **86**: 524-538.

Erhardt, M. (2016) Strategies to block bacterial pathogenesis by interference with motility and chemotaxis. *Curr. Top. Microbiol. Immunol.* **398**: 185-205.

Faigenbaum-Romm, R., Reich, A., Gatt, Y.E., Barsheshet, M., Argaman, L., and Margalit, H. (2020) Hierarchy in Hfq chaperon occupancy of small RNA targets plays a major role in their regulation. *Cell Rep.* **30**: 3127-3138.e3126.

Fitzgerald, D.M., Bonocora, R.P., and Wade, J.T. (2014) Comprehensive mapping of the *Escherichia coli* flagellar regulatory network. *PLoS Genet.* **10**: e1004649.

Fitzgerald, D.M., Smith, C., Lapierre, P., and Wade, J.T. (2018) The evolutionary impact of intragenic FliA promoters in proteobacteria. *Mol. Microbiol.* **108**: 361-378.

Freedman, L.P., Zengel, J.M., Archer, R.H., and Lindahl, L. (1987) Autogenous control of the S10 ribosomal protein operon of *Escherichia coli*: genetic dissection of transcriptional and posttranscriptional regulation. *Proc. Natl. Acad. Sci. USA* **84**: 6516-6520.

Guo, M.S., Updegrove, T.B., Gogol, E.B., Shabalina, S.A., Gross, C.A., and Storz, G. (2014) MicL, a new σE-dependent sRNA, combats envelope stress by repressing synthesis of Lpp, the major outer membrane lipoprotein. *Genes Dev.* **28**: 1620-1634.

Guttenplan, S.B., and Kearns, D.B. (2013) Regulation of flagellar motility during biofilm formation. *FEMS Microbiol. Rev.* **37**: 849-871.

Guzman, L.M., Belin, D., Carson, M.J., and Beckwith, J. (1995) Tight regulation, modulation, and high-level expression by vectors containing the arabinose P_{BAD} promoter. *J. Bacteriol.* **177**: 4121-4130.

Holmqvist, E., and Vogel, J. (2018) RNA-binding proteins in bacteria. *Nat. Rev. Microbiol.* **16**: 601-615.

Hör, J., Matera, G., Vogel, J., Gottesman, S., and Storz, G. (2020) Trans-acting small RNAs and their effects on gene expression in *Escherichia coli* and *Salmonella enterica*. *EcoSal Plus* **9**: doi: 10.1128/ecosalplus.ESP-0030-2019.

Huang da, W., Sherman, B.T., and Lempicki, R.A. (2009) Systematic and integrative analysis of large gene lists using DAVID bioinformatics resources. *Nat. Protoc.* **4**: 44-57.

Ikeda, T., Homma, M., Iino, T., Asakura, S., and Kamiya, R. (1987) Localization and stoichiometry of hook-associated proteins within *Salmonella typhimurium* flagella. *J. Bacteriol.* **169**: 1168-1173.

Kalir, S., Mangan, S., and Alon, U. (2005) A coherent feed-forward loop with a SUM input function prolongs flagella expression in *Escherichia coli*. *Mol Syst Biol* **1**: 2005.0006.

Kalir, S., McClure, J., Pabbaraju, K., Southward, C., Ronen, M., Leibler, S., Surette, M.G., and Alon, U. (2001) Ordering genes in a flagella pathway by analysis of expression kinetics from living bacteria. *Science* **292**: 2080-2083.

Kearns, D.B. (2010) A field guide to bacterial swarming motility. *Nat. Rev. Microbiol.* **8**: 634-644.

Kent, W.J., Sugnet, C.W., Furey, T.S., Roskin, K.M., Pringle, T.H., Zahler, A.M., and Haussler, D. (2002) The human genome browser at UCSC. *Genome Res.* **12**: 996-1006.

Keseler, I.M., Mackie, A., Peralta-Gil, M., Santos-Zavaleta, A., Gama-Castro, S., Bonavides-Martínez, C., Fulcher, C., Huerta, A.M., Kothari, A., Krummenacker, M., Latendresse, M., Muñiz-Rascado, L., Ong, Q., Paley, S., Schröder, I., Shearer, A.G., Subhraveti, P., Travers, M., Weerasinghe, D., Weiss, V., Collado-Vides, J., Gunsalus, R.P., Paulsen, I., and Karp, P.D. (2013) EcoCyc: fusing model organism databases with systems biology. *Nucleic Acids Res.* **41**: D605-D612.

Landini, P., and Zehnder, A.J. (2002) The global regulatory hns gene negatively affects adhesion to solid surfaces by anaerobically grown *Escherichia coli* by modulating expression of flagellar genes and lipopolysaccharide production. *J. Bacteriol.* **184**: 1522-1529.

Lehnen, D., Blumer, C., Polen, T., Wackwitz, B., Wendisch, V.F., and Unden, G. (2002) LrhA as a new transcriptional key regulator of flagella, motility and chemotaxis genes in *Escherichia coli*. *Mol. Microbiol.* **45**: 521-532.

Luo, X., Hsiao, H.H., Bubunenko, M., Weber, G., Court, D.L., Gottesman, M.E., Urlaub, H., and Wahl, M.C. (2008) Structural and functional analysis of the *E. coli* NusB-S10 transcription antitermination complex. *Mol. Cell* **32**: 791-802.

Lüttgen, H., Robelek, R., Mühlberger, R., Diercks, T., Schuster, S.C., Köhler, P., Kessler, H., Bacher, A., and Richter, G. (2002) Transcriptional regulation by antitermination. Interaction of RNA with NusB protein and NusB/NusE protein complex of *Escherichia coli*. *J. Mol. Biol.* **316**: 875-885.

Marger, M.D., and Saier, M.H.J. (1993) A major superfamily of transmembrane facilitators that catalyse uniport, symport and antiport. *Trends Biochem. Sci.* **18**: 13-20.

Melamed, S. (2020) New sequencing methodologies reveal interplay between multiple RNA-binding proteins and their RNAs. *Curr. Genet.* **66**: 713-717.

Melamed, S., Adams, P.P., Zhang, A., Zhang, H., and Storz, G. (2020) RNA-RNA interactomes of ProQ and Hfq reveal overlapping and competing roles. *Mol. Cell* **77**: 411-425.

Melamed, S., Faigenbaum-Romm, R., Peer, A., Reiss, N., Shechter, O., Bar, A., Altuvia, Y., Argaman, L., and Margalit, H. (2018) Mapping the small RNA interactome in bacteria using RIL-seq. *Nat. Protoc.* **13**: 1-33.

Melamed, S., Peer, A., Faigenbaum-Romm, R., Gatt, Y.E., Reiss, N., Bar, A., Altuvia, Y., Argaman, L., and Margalit, H. (2016) Global mapping of small RNA-target interactions in bacteria. *Mol. Cell* **63**: 884-897.

Nakamura, S., and Minamino, T. (2019) Flagella-driven motility of bacteria. *Biomolecules* **9**: 279.

Osterman, I.A., Dikhtyar, Y.Y., Bogdanov, A.A., Dontsova, O.A., and Sergiev, P.V. (2015) Regulation of flagellar gene expression in bacteria. *Biochemistry (Mosc.)* **80**: 1447-1456.

Papenfort, K., and Vanderpool, C.K. (2015) Target activation by regulatory RNAs in bacteria. *FEMS Microbiol. Rev.* **39**: 362-378.

Pesavento, C., Becker, G., Sommerfeldt, N., Possling, A., Tschowri, N., Mehlis, A., and Hengge, R. (2008) Inverse regulatory coordination of motility and curli-mediated adhesion in *Escherichia coli*. *Genes Dev.* **22**: 2434-2446.

Prüß, B.M. (2017) Involvement of two-component signaling on bacterial motility and biofilm development. *J. Bacteriol.* **199**: e00259-00217.

Shi, W., Li, C., Louise, C.J., and Adler, J. (1993) Mechanism of adverse conditions causing lack of flagella in *Escherichia coli*. *J. Bacteriol.* **175**: 2236-2240.

Smith, T.G., and Hoover, T.R. (2009) Deciphering bacterial flagellar gene regulatory networks in the genomic era. *Adv. Appl. Microbiol.* **67**: 257-295.

Soutourina, O.A., and Bertin, P.N. (2003) Regulation cascade of flagellar expression in Gram-negative bacteria. *FEMS Microbiol. Rev.* **27**: 505-523.

Streit, S., Michalski, C.W., Erkan, M., Kleeff, J., and Friess, H. (2009) Northern blot analysis for detection and quantification of RNA in pancreatic cancer cells and tissues. *Nat. Protoc.* **4**: 37-43.

Stringer, A.M., Singh, N., Yermakova, A., Petrone, B.L., Amarasinghe, J.J., Reyes-Diaz, L., Mantis, N.J., and Wade, J.T. (2012) FRUIT, a scar-free system for targeted chromosomal mutagenesis, epitope tagging, and promoter replacement in *Escherichia coli* and *Salmonella enterica*. *PLoS One* **7**: e44841.

Thomason, M.K., Bischler, T., Eisenbart, S.K., Förstner, K.U., Zhang, A., Herbig, A., Nieselt, K., Sharma, C.M., and Storz, G. (2015) Global transcriptional start site mapping using differential RNA sequencing reveals novel antisense RNAs in *Escherichia coli*. *J. Bacteriol.* **197**: 18-28.

Thomason, M.K., Fontaine, F., De Lay, N., and Storz, G. (2012) A small RNA that regulates motility and biofilm formation in response to changes in nutrient availability in *Escherichia coli*. *Mol. Microbiol.* **84**: 17-35.

Thomson, N.M., Rossmann, F.M., Ferreira, J.L., Matthews-Palmer, T.R., Beeby, M., and Pallen, M.J. (2018) Bacterial flagellins: does size matter? *Trends Microbiol.* **26**: 575-581.

Typas, A., Barembruch, C., Possling, A., and Hengge, R. (2007) Stationary phase reorganisation of the *Escherichia coli* transcription machinery by Crl protein, a fine-tuner of sigmas activity and levels. *EMBO J.* **26**: 1569-1578.

Updegrove, T.B., Zhang, A., and Storz, G. (2016) Hfq: the flexible RNA matchmaker. *Curr. Opin. Microbiol.* **30**: 133-138.

Urban, J.H., and Vogel, J. (2009) A green fluorescent protein (GFP)-based plasmid system to study post-transcriptional control of gene expression in vivo. *Methods Mol. Biol.* **540**: 301-319.

Verhamme, D.T., Arents, J.C., Postma, P.W., Crielaard, W., and Hellingwerf, K.J. (2001) Glucose-6-phosphate-dependent phosphoryl flow through the Uhp two-component regulatory system. *Microbiology* **147**: 3345-3352.

Westermann, A.J., Venturini, E., Sellin, M.E., Förstner, K.U., Hardt, W.-D., and Vogel, J. (2019) The major RNA-binding protein ProQ impacts virulence gene expression in *Salmonella enterica* serovar Typhimurium. *mBio* **10**: e02504-02518.

Zeghouf, M., Li, J., Butland, G., Borkowska, A., Canadien, V., Richards, D., Beattie, B., Emili, A., and Greenblatt, J.F. (2004) Sequential Peptide Affinity (SPA) system for the identification of mammalian and bacterial protein complexes. *J. Proteome Res.* **3**: 463-468.

Zengel, J.M., and Lindahl, L. (1992) Ribosomal protein L4 and transcription factor NusA have separable roles in mediating terminating of transcription within the leader of the S10 operon of *Escherichia coli*. *Genes Dev.* **6**: 2655-2662.

Zengel, J.M., and Lindahl, L. (1996) A hairpin structure upstream of the terminator hairpin required for ribosomal protein L4-mediated attenuation control of the S10 operon of *Escherichia coli*. *J. Bacteriol.* **178**: 2383-2387.

Zengel, J.M., Sha, Y., and Lindahl, L. (2002) Surprising flexibility of leader RNA determinants for r-protein L4-mediated transcription termination in the *Escherichia coil* S10 operon. *RNA Biol.* **8**: 572-578.

Zhang, A., Altuvia, S., Tiwari, A., Argaman, L., Hengge-Aronis, R., and Storz, G. (1998) The OxyS regulatory RNA represses *rpoS* translation and binds the Hfq (HF-I) protein. *EMBO J.* **17**: 6061-6068.

Zhang, A., Schu, D.J., Tjaden, B.C., Storz, G., and Gottesman, S. (2013a) Mutations in interaction surfaces differentially impact *E. coli* Hfq association with small RNAs and their mRNA targets. *J. Mol. Biol.* **425**: 3678-3697.

Zhang, A., Wassarman, K.M., Ortega, J., Steven, A.C., and Storz, G. (2002) The Sm-like Hfq protein increases OxyS RNA interaction with target mRNAs. *Mol. Cell* **9**: 11-22.

Zhang, H., Meltzer, P., and Davis, S. (2013b) RCircos: an R package for Circos 2D track plots. *BMC Bioinformatics* **14**: 244.

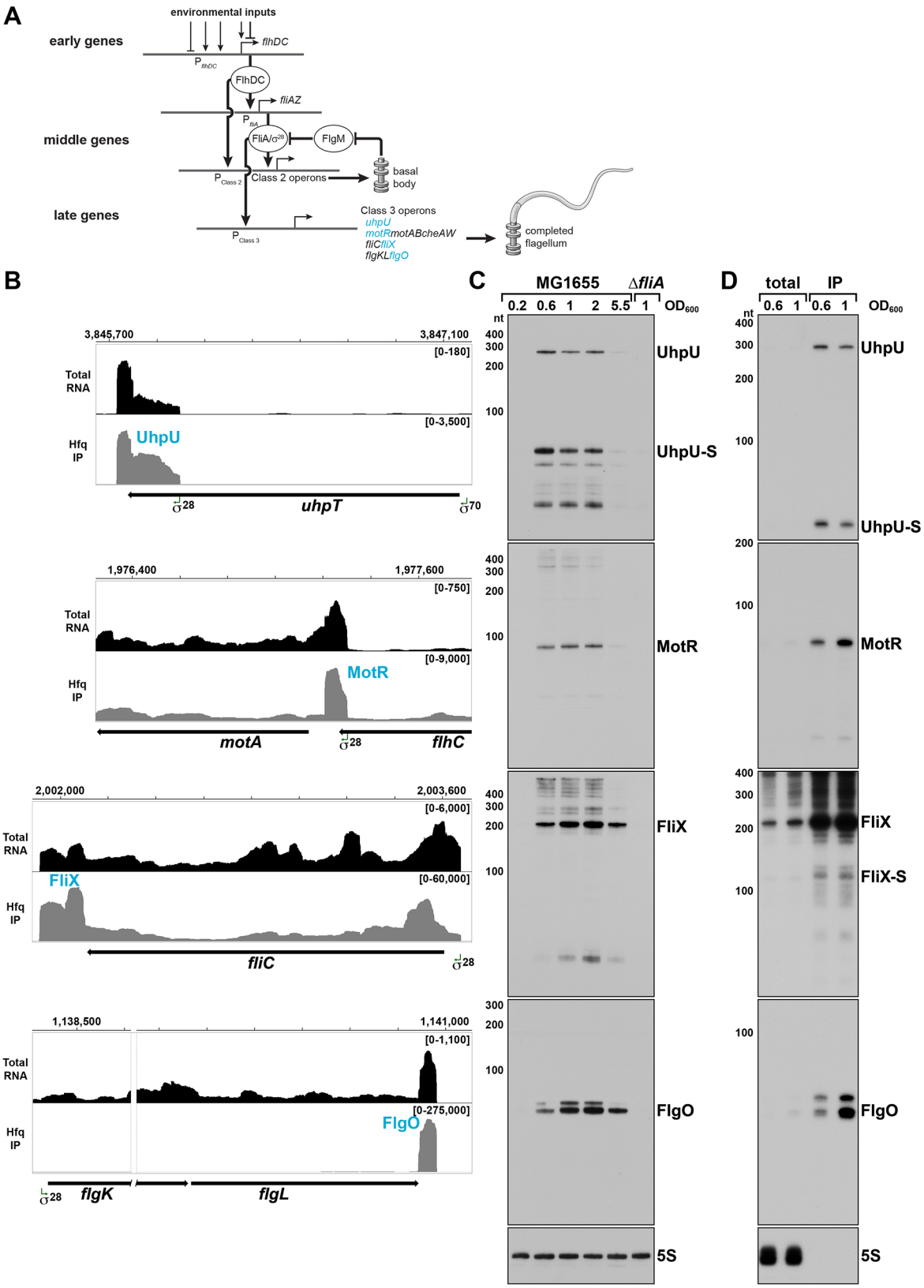
A
environmental inputs
early genes
flhDC
FlhDC
fliAZ
middle genes
FliA/σ28
FlgM
basal body
Class 2 operons
late genes
Class 3 operons
uhpU
motRmotABcheAW
fliCfliX
flgKLflgO
completed flagellum
B
3,845,700
3,847,100
Total RNA
Hfq IP
UhpU
uhpT
1,976,400
1,977,600
MotR
motA
flhC
2,002,000
2,003,600
FliX
fliC
1,138,500
1,141,000
FlgO
flgK
flgL
C
MG1655
ΔfliA
0.2 0.6 1 2 5.5 1
OD600
nt
UhpU
UhpU-S
MotR
FliX
FlgO
5S
D
total
IP
0.6 1 0.6 1
FliX-S

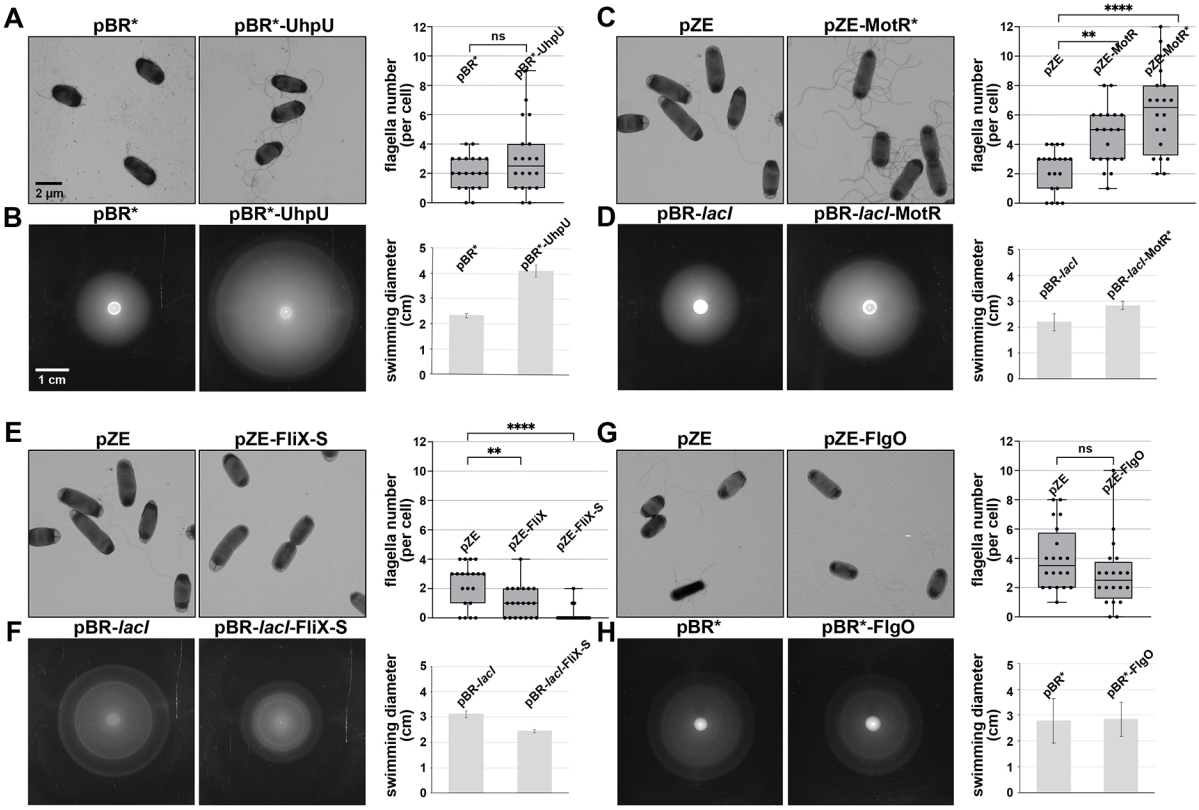
A
pBR*
pBR*-UhpU
2 µm
ns
pBR*
pBR*-UhpU
flagella number (per cell)
B
pBR*
pBR*-UhpU
1 cm
pBR*
pBR*-UhpU
swimming diameter (cm)
C
pZE
pZE-MotR*
****
**
pZE
pZE-MotR
pZE-MotR*
flagella number (per cell)
D
pBR-lacI
pBR-lacI-MotR
pBR-lacI
pBR-lacI-MotR*
swimming diameter (cm)
E
pZE
pZE-FliX-S
****
**
pZE
pZE-FliX
pZE-FliX*-S
flagella number (per cell)
F
pBR-lacI
pBR-lacI-FliX-S
pBR-lacI
pBR-lacI-FliX-S
swimming diameter (cm)
G
pZE
pZE-FlgO
ns
pZE
pZE-FlgO
flagella number (per cell)
H
pBR*
pBR*-FlgO
pBR*
pBR*-FlgO
swimming diameter (cm)

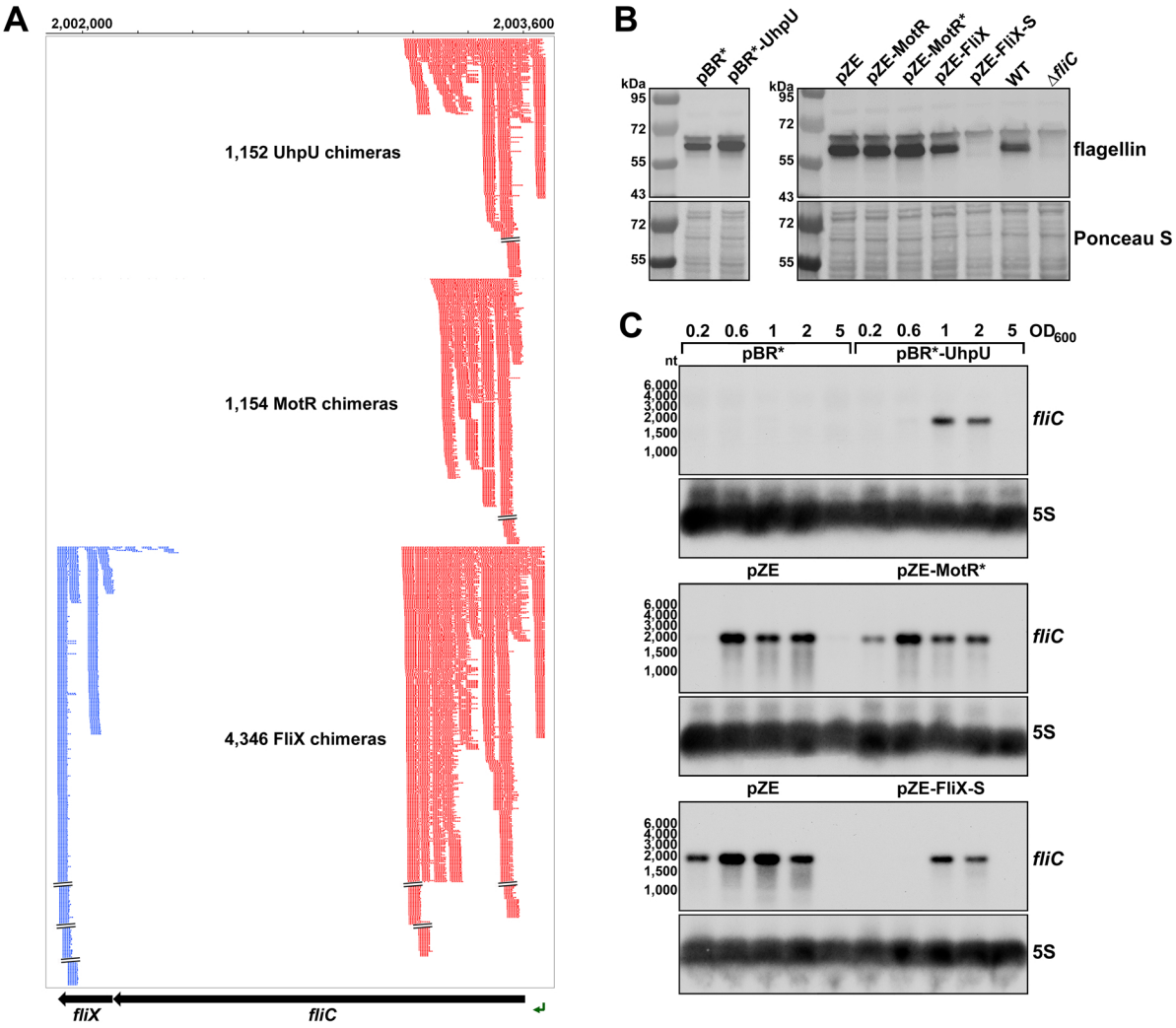
A
2,002,000
2,003,600
1,152 UhpU chimeras
1,154 MotR chimeras
4,346 FliX chimeras
fliX
fliC
B
pBR*
pBR*-UhpU
kDa
95
72
55
43
72
55
pZE
pZE-MotR
pZE-MotR*
pZE-FliX
pZE-FliX-S
WT
ΔfliC
flagellin
Ponceau S
C
0.2 0.6 1 2 5 0.2 0.6 1 2 5 OD600
pBR*
pBR*-UhpU
nt
6,000
4,000
3,000
2,000
1,500
1,000
fliC
5S
pZE
pZE-MotR*
pZE-FliX-S

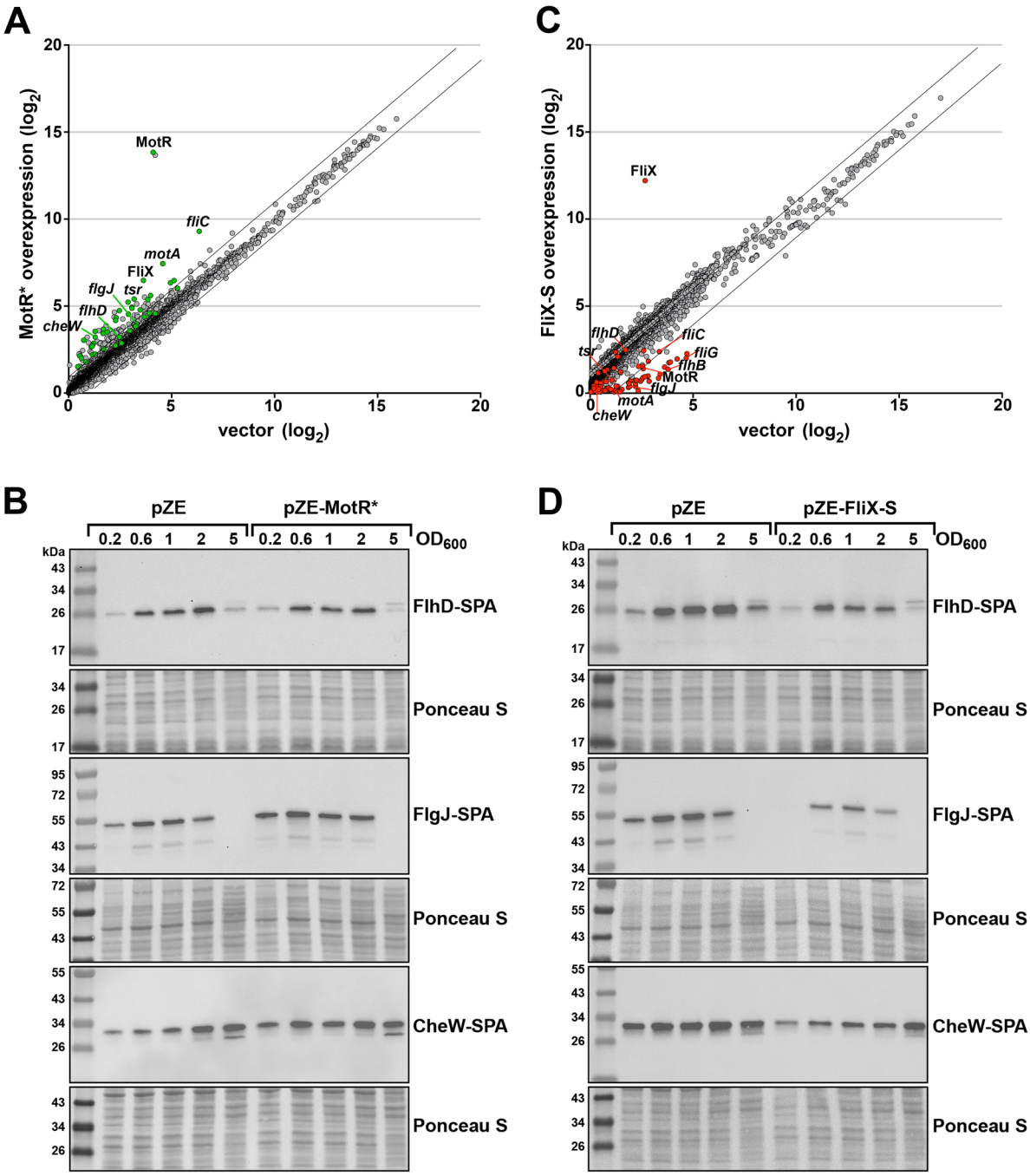
A
MotR* overexpression (log2)
vector (log2)
MotR
fliC
motA
FliX
flgJ
tsr
flhD
cheW
C
FliX-S overexpression (log2)
vector (log2)
FliX
flhD
tsr
fliC
fliG
flhB
MotR
flgJ
motA
cheW
B
pZE
pZE-MotR*
0.2 0.6 1 2 5 0.2 0.6 1 2 5
OD600
kDa
FlhD-SPA
Ponceau S
FlgJ-SPA
Ponceau S
CheW-SPA
Ponceau S
D
pZE
pZE-FliX-S
0.2 0.6 1 2 5 0.2 0.6 1 2 5
OD600
kDa
FlhD-SPA
Ponceau S
FlgJ-SPA
Ponceau S
CheW-SPA
Ponceau S

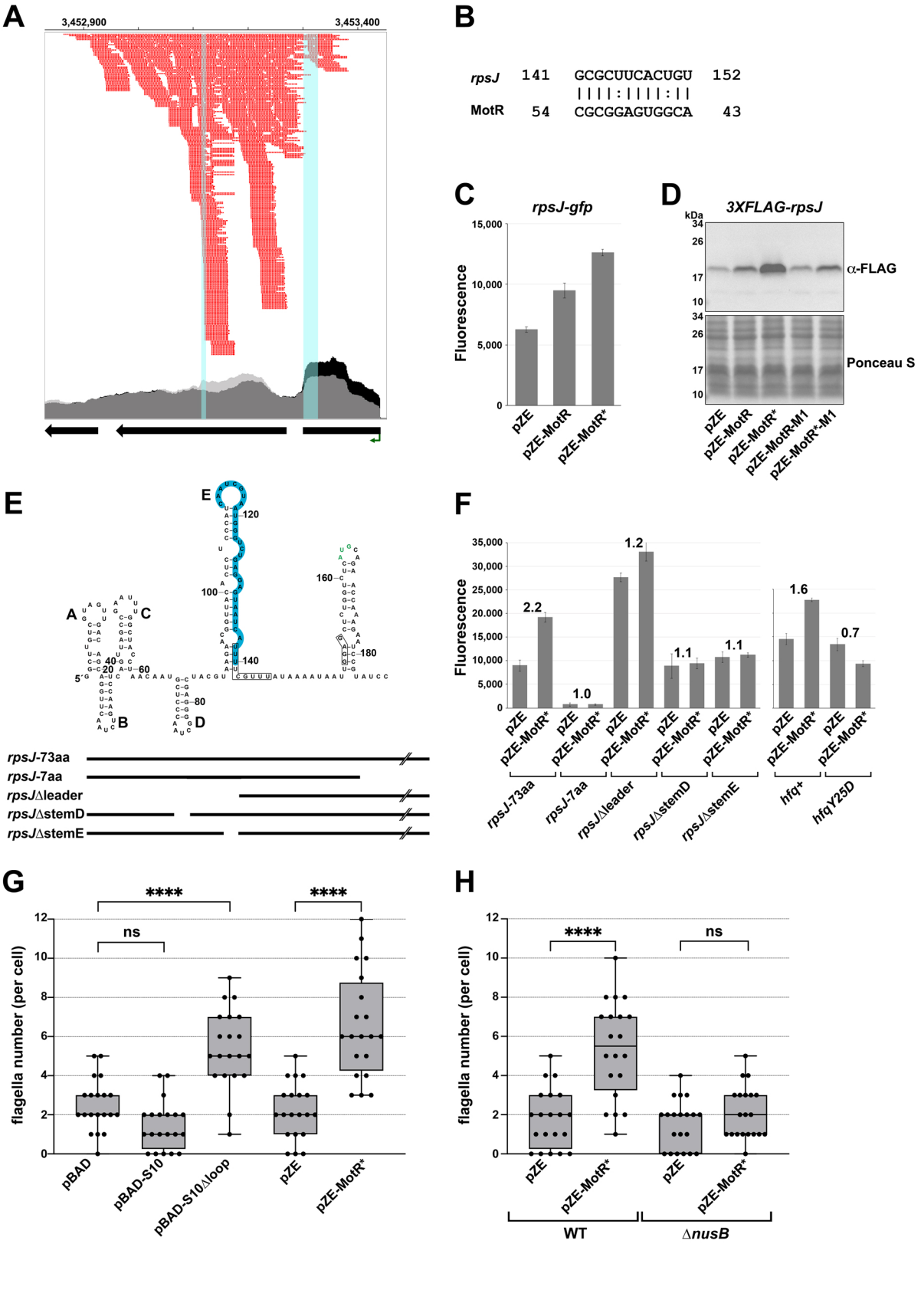
A
3,452,900
3,453,400
B
rpsJ 141 GCGCUUCACUGU 152
MotR 54 CGCGGAGUGGCA 43
C
rpsJ-gfp
Fluorescence
15,000
10,000
5,000
0
pZE
pZE-MotR
pZE-MotR*
D
3XFLAG-rpsJ
kDa
34
26
17
10
α-FLAG
Ponceau S
pZE
pZE-MotR
pZE-MotR*
pZE-MotR-M1
pZE-MotR*-M1
E
A
B
C
D
E
rpsJ-73aa
rpsJ-7aa
rpsJΔleader
rpsJΔstemD
rpsJΔstemE
F
Fluorescence
35,000
30,000
25,000
20,000
15,000
10,000
5,000
0
2.2
1.0
1.2
1.1
1.1
1.6
0.7
pZE
pZE-MotR*
rpsJ-73aa
rpsJ-7aa
rpsJΔleader
rpsJΔstemD
rpsJΔstemE
hfq+
hfqY25D
G
flagella number (per cell)
****
ns
****
pBAD
pBAD-S10
pBAD-S10Δloop
pZE
pZE-MotR*
H
flagella number (per cell)
****
ns
pZE
pZE-MotR*
WT
ΔnusB

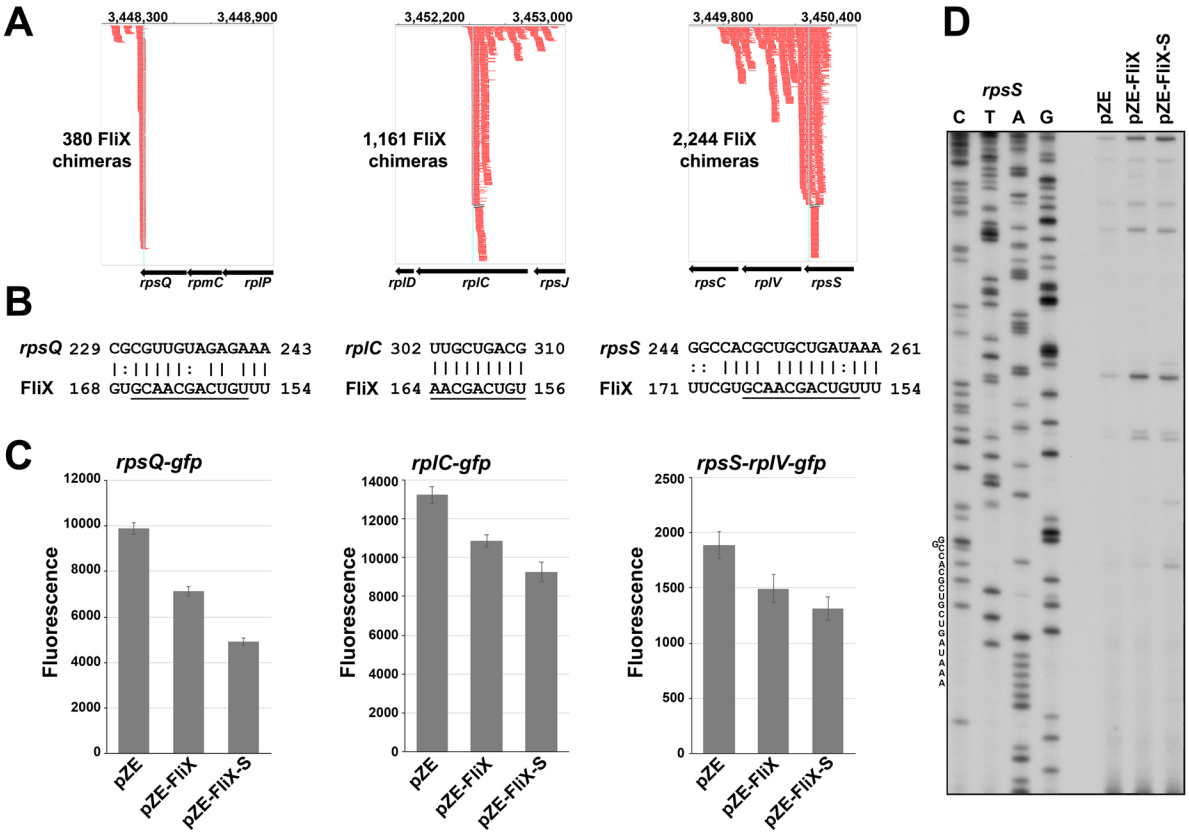
A
3,448,300
3,448,900
380 FliX chimeras
rpsQ
rpmC
rplP
3,452,200
3,453,000
1,161 FliX chimeras
rplD
rplC
rpsJ
3,449,800
3,450,400
2,244 FliX chimeras
rpsC
rplV
rpsS
B
rpsQ 229 CGCGUUGUAGAGAAA 243
FliX 168 GUGCAACGACUGUUU 154
rplC 302 UUGCUGACG 310
FliX 164 AACGACUGU 156
rpsS 244 GGCCACGCUGCUGAUAAA 261
FliX 171 UUCGUGCAACGACUGUUU 154
C
rpsQ-gfp
rplC-gfp
rpsS-rplV-gfp
Fluorescence
pZE
pZE-FliX
pZE-FliX-S
D
rpsS
C T A G
pZE
pZE-FliX
pZE-FliX-S

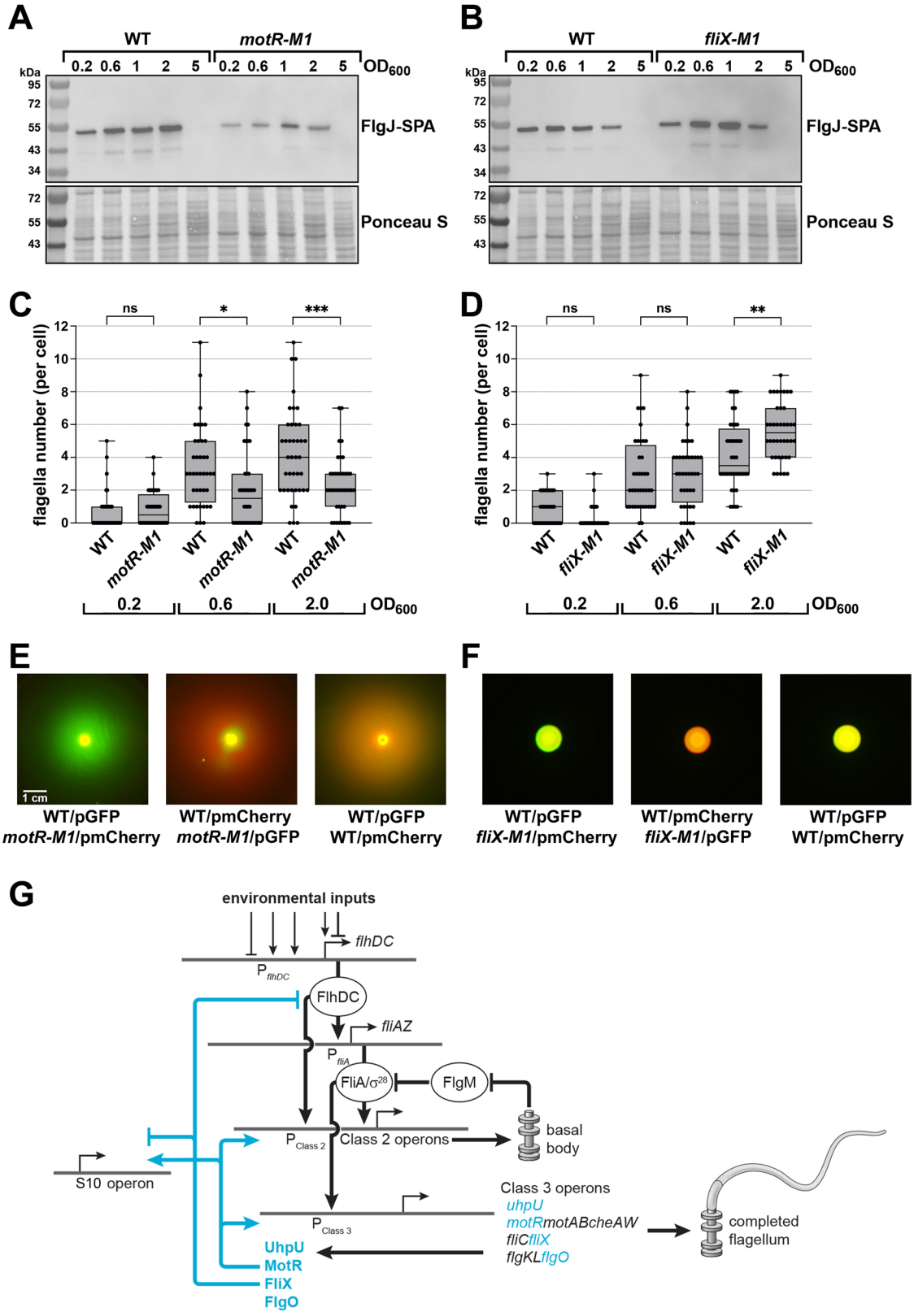
A
WT
motR-M1
0.2 0.6 1 2 5 0.2 0.6 1 2 5
OD600
kDa
95
72
55
43
34
FlgJ-SPA
72
55
43
Ponceau S
B
WT
fliX-M1
0.2 0.6 1 2 5 0.2 0.6 1 2 5
OD600
FlgJ-SPA
Ponceau S
C
ns
*
***
flagella number (per cell)
WT
motR-M1
0.2
0.6
2.0
OD600
D
ns
ns
**
fliX-M1
E
1 cm
WT/pGFP
motR-M1/pmCherry
WT/pmCherry
motR-M1/pGFP
WT/pGFP
WT/pmCherry
F
WT/pGFP
fliX-M1/pmCherry
WT/pmCherry
fliX-M1/pGFP
WT/pGFP
WT/pmCherry
G
environmental inputs
flhDC
P flhDC
FlhDC
fliAZ
P fliA
FliA/σ28
FlgM
basal
body
P Class 2
Class 2 operons
S10 operon
Class 3 operons
uhpU
motRmotABcheAW
fliCfliX
flgKLflgO
P Class 3
completed
flagellum
UhpU
MotR
FliX
FlgO